Compound-specific stable carbon and hydrogen isotope analyses of Late-Holocene vegetation and precipitation change at Laguna Los Mangos, Costa Rica

Elizabeth A. Yanuskiewicz[a], Chad S. Lane[a,*], Sally P. Horn[b], Erik N. Johanson[c], Douglas W. Gamble[a]

[a] Department of Earth and Ocean Sciences, University of North Carolina Wilmington, Wilmington, NC 28403, USA

[b] Department of Geography, University of Tennessee, Knoxville, TN 37996, USA

[c] Department of Geosciences, Florida Atlantic University, Boca Raton, FL 33431 USA

* Corresponding author

E-mail address: lanec@uncw.edu (C. Lane).

Abstract

New compound-specific isotope analyses of a sediment core from Laguna Los Mangos in southern Pacific Costa Rica improves understanding of late-Holocene precipitation change in a region with limited paleoprecipitation records that is vulnerable to future climate change. We established paleoprecipitation and paleovegetation records from compound-specific stable hydrogen and carbon isotopic compositions of terrestrially-derived *n*-alkanes (δ^2H_{alkane} and $\delta^{13}C_{alkane}$) to assess paleohydrologic variability and potential linkages to paleoecological change and human activity as revealed by prior analyses of the Los Mangos core. The δ^2H_{alkane} values were corrected for isotopic fractionation using pollen counts from the same core. The Los Mangos record extends to 4200 cal yr BP and small increases in $\delta^{13}C$ values of C_{29}, +0.6‰, and C_{31} alkanes, +0.3‰, ($\delta^{13}C_{C29, 31}$) indicate a slight increase in C_4 vegetation after initial introduction of maize agriculture to the watershed at ca. 3360 cal yr BP. This slight increase in C_4 vegetation is followed by the largest positive carbon isotope excursions in the record, as compared to record averages ($\delta^{13}C_{C29}$ = +3.2‰, $\delta^{13}C_{C31}$ = +5.0‰). Paleohydrologic variability likely influenced vegetation and human activity at Los Mangos. Lake desiccation during the late-Terminal Classic Drought (TCD) resulted in a sedimentary hiatus in the Los Mangos record from ca. 950 to 450 cal yr BP. Positive excursions in comparison to record averages occur for both δ^2H_{C29} and δ^2H_{C31} proxies (δ^2H_{C29} = +25.3 to +13.4‰ and δ^2H_{C31} = +6.5‰) during the middle Little Ice Age (LIA) and indicate drier than average conditions, but there is no evidence of desiccation during this period. Thus, drought conditions during the LIA were apparently not as severe at Los Mangos as during the TCD, possibly because of differing forcing mechanisms for LIA climate that originated, or were more clearly expressed, in the Atlantic basin.

Keywords: Hydrogen isotopes; Carbon isotopes; Terminal Classic Drought; Little Ice Age; Ocean-atmospheric dynamics; Costa Rica

1.0 Introduction

Sedimentary records of past climate variability and prehistoric human-environment interactions offer temporally-unique insights into the range of climate variability, the evolution of complex ecological systems, and the response of human populations to environmental stressors (Bhattacharya et al., 2015; Haug et al., 2003; Hodell et al., 2005; Kerr et al., 2020; Lane et al., 2014). Understanding how natural and human systems respond to climatic stress on decadal to centennial timescales is particularly important with projected increases in the amplitude and duration of extreme climate conditions over the coming decades (Magrin et al., 2014). Periods of time with spatially and temporally robust proxy evidence for anomalous regional climate conditions such as the Terminal Classic Drought (TCD; 1200 to 850 cal yr BP) or Little Ice Age (LIA; 500 to 100 cal yr BP) offer particularly good case studies that, in combination, can also be used to isolate potential climate forcing mechanisms. Bhattacharya et al. (2017) and Wu et al. (2019) compiled climate proxy records during the TCD and Lane et al. (2011a) compiled records during the LIA that document drought in the circum-Caribbean to discuss specific climate forcing mechanisms that may have caused regional droughts. However, those studies demonstrated a lack of records from sites on the Pacific slope of Middle America or with precipitation regimes controlled primarily by atmospheric forcing mechanisms associated with the Pacific Ocean. Such records are required to isolate potential climate forcing mechanisms

for the circum-Caribbean because of the region's sensitivity to both Atlantic and Pacific climate dynamics (Giannini et al., 2001).

Laguna Los Mangos (Los Mangos) is a freshwater lake on the Pacific slope of Costa Rica in the Térraba River basin, where the precipitation regime is strongly linked to Pacific ocean-atmospheric dynamics such as the El Niño-Southern Oscillation (ENSO; George et al., 1998; Krishnaswamy et al., 2001). Johanson et al. (2019) analyzed the Los Mangos sediment core for pollen, charcoal, and bulk sediment geochemistry to interpret the timing and spatial variability of pre-Columbian land use and modification. Pollen analysis of the Los Mangos core indicated that the site supported tropical moist forest dominated by C_3 plants prior to forest clearance for prehistoric maize agriculture (Johanson et al., 2019). Maize pollen first appears in the Los Mangos sedimentary record around 3360 cal yr BP and persists until the early TCD (1170 cal yr BP), signaling continual agricultural activity and the expansion of C_4 plants. $\delta^{13}C_{TOC}$ values remain above the profile mean after 3360 cal yr BP until the middle LIA, offering some insight on the scale of vegetation change to the area, which is not possible by analyzing pollen alone. The $\delta^{13}C_{TOC}$ record is particularly valuable for estimating the scale of past maize cultivation. Maize pollen disperses only short distances (Raynor et al., 1972), and is typically rare in sediment cores even when present (Horn, 2006), such that pollen percentages may not be sensitive to the extent of maize agriculture in watersheds (Taylor et al., 2013). The addition of $\delta^{13}C_{TOC}$ values assists in detecting dominant photosynthetic pathways through the Los Mangos record, allowing for interpretations of vegetation replacement due to agricultural activities even if maize pollen counts are low (Lane et al., 2009a). Johanson et al. (2019) hypothesized that extreme drought and associated decreases in lake level during the early TCD would have significantly affected maize agriculture around Los Mangos due to decreased water availability.

Agriculture proxies such as $\delta^{13}C_{TOC}$, charcoal area influx, carbon to nitrogen ratios (C:N), and percent organic matter (%OM) all show decreasing values just after ca. 1170 cal yr BP and extending through the LIA and Spanish arrival (Johanson et al., 2019). No data are available for the period 950–450 cal yr BP, when drought resulted in a hiatus in the sediment profile (Johanson et al., 2019). Johanson et al. (2019) concluded that severe aridity during the late TCD, aridity during the LIA, and population decline from the spread of disease following the Spanish Conquest drove declines in agricultural activity around Los Mangos until the twentieth century. However, bulk sediment isotope and pollen datasets can be ambiguous when trying to isolate natural vs. anthropogenic changes in the environment. The addition of more diagnostic compound-specific isotope proxies at Los Mangos could improve our understanding of regional climate variability and the response of both natural and anthropogenic systems to such variability through time. Analyzing $\delta^{13}C_{alkane}$ and $\delta^{2}H_{alkane}$ proxies can reveal how climatic events influenced Los Mangos and how such events may have affected human occupation, as previously explored by Johanson et al. (2019) based on bulk stable isotopes, charcoal, and pollen.

In this study, we apply carbon and hydrogen isotope analyses of terrestrially-derived *n*-alkanes to the Los Mangos sediment core to assess whether clear linkages exist between paleoprecipitation dynamics, vegetation change, and agricultural activity over the Late Holocene. We also investigate the expression of the TCD and LIA on the Pacific slope of southern Costa Rica to better understand potential forcing mechanisms for extended drought events in this region of scarce studies.

2.0 Regional setting

115 *2.1*

116 *Laguna Los Mangos*

117 Los Mangos (9.0894 N, 83.4666 W) is a 0.3 ha, closed basin freshwater lake located at
118 475 m elevation in the Fila Costeña of southern Pacific Costa Rica. The Los Mangos basin
119 appears to have formed from a landslide around 4300 cal yr BP and has a maximum water depth
120 of 0.5 m (Johanson et al., 2019). Johanson et al. (2019) retrieved a sediment core 752 cm long in
121 2014 near the center of Los Mangos; all prior and compound-specific (this study) proxies are
122 derived from this sediment core.

123 Los Mangos is located within the Diquís subregion of the Gran Chiriquí archaeological
124 region of southern Pacific Costa Rica and western Panama. The major cultural periods of the
125 Diquís subregion document the transformation from hunter-gathers to a complex hierarchical
126 society with large populations dependent on maize agriculture (Corrales, 2000). The latest
127 period, the Chiriquí period, ended with the Spanish Conquest, when the Chiriquí lost an
128 estimated 90–95% of its population (Dobyns, 1966).

129 Sediment cores have been analyzed from several other lakes in the Diquís subregion:
130 Laguna Zoncho cores spanning 3600 cal yr BP to present (Clement and Horn, 2001; Lane et al.,
131 2004; Taylor et al., 2013; Taylor et al., 2020), Santa Elena spanning ca. 1950 cal yr BP to present
132 (Anchukaitis and Horn, 2005; Kerr et al., 2020), Vueltas spanning from at least 1200 cal yr BP to
133 present (Horn and Haberyan, 2016), and Gamboa from 2500 cal yr BP to present (Horn, 2006)
134 are located in the southeastern part of the Diquís subregion, and their records begin at or after the
135 arrival of maize agriculture (Figure 1, top; Horn, 2006). Lagunas Danta (ca. 800 cal yr to
136 present) and Carse (ca. 350 cal yr BP to present) (Johanson et al., 2020) are located near Los
137 Mangos in the western part of the Diquís subregion, but their records cover less than 800 years,

beginning well after the arrival of maize agriculture. Only Los Mangos in the western Diquís has a record that begins prior to the establishment of maize agriculture, establishing a baseline for the natural environment (Johanson et al., 2019).

2.1.1 Present regional precipitation dynamics

Precipitation dynamics in Central America are influenced by multiple forcing mechanisms related to latitudinal position, isthmian geography, and topography. Southern Pacific Costa Rica receives 2500–5000 mm precipitation annually (Instituto Meteorológico Nacional), with a rainy season from May to October (Sánchez-Murillo et al., 2016). Generally, the descending branch of the Hadley cell controls regional circulation. The trade winds dominate low-level circulation during the dry season (November–April, Durán-Quesada et al., 2020) with dominant easterly flow reducing precipitation along the Pacific coast of Costa Rica, because of rain shadowing and intensification of the easterly Caribbean Low-Level Jet (Wang, 2007; Hidalgo et al., 2019). In the wet season, the northward migration of the Pacific limb of the ITCZ decreases trade wind intensities and creates cross-equatorial winds that recurve to become southwesterly and transport Pacific moisture into southwestern Costa Rica via the westerly Chorro del Occidente Colombiano (CHOCO) jet that does not typically penetrate past the Cordillera (Sánchez-Murillo et al., 2016). Numerous anomalous events may disrupt normal state conditions for Costa Rica, one major influencing anomalous event is the El Nino-Southern Oscillation (ENSO) originating in the tropical Pacific.

ENSO events can be termed either cold “La Niña” or warm “El Niño” events. Cold and warm events are fundamentally different, and all events differ from one another (Sarachik and Cane, 2010). ENSO is mainly controlled by anomalous heating in the central and eastern

equatorial Pacific, which develops a zonal seesaw in sea level pressure between the eastern equatorial Pacific and the tropical Atlantic. Lower than average sea level pressures occur in the eastern equatorial Pacific with higher than average sea level pressures in the tropical Atlantic (Curtis and Hastenrath, 1995; Hastenrath and Heller, 1977; Covey and Hastenrath, 1978; Poveda and Mesa, 1997; Giannni et al., 2001). Drier than average conditions occur in the Caribbean Basin during July-October of the first year of a warm ENSO event due to divergence in the basin (Ropelewski and Halpert, 1987, 1996). During dry years the velocity and duration of the northeast trade winds and associated Caribbean Low-Level Jet increase over the Caribbean because of opposing signs of pressure in the North Atlantic and the eastern equatorial Pacific (Hastenrath and Lamb, 1977; Waylen and Laporte, 1999; Bhattacharya et al., 2017). This trade wind dynamic results in increased precipitation on the Caribbean slope of Costa Rica from onshore flow of northeast trade winds (Vargas and Trejos, 1994), while the Pacific slope of Costa Rica, which lies in the rain shadow, experiences lower rainfall than the Caribbean slope because of the significant orographic effect of the central highlands (Vargas and Trejos, 1994). Additionally, Pulwarty and Diaz (1993) found during warm ENSO events the eastern equatorial Pacific intertropical convergence zone (ITCZ) shifts to a south-west position, which would also inhibit convection and decrease rainfall along the Pacific slope of Costa Rica (Durán-Quesada et al., 2020).

Pacific Ocean dynamics most directly influence the precipitation regime around Los Mangos today, with ENSO as one of the strongest controls on inter-annual precipitation variability in the Térraba watershed (George et al., 1998; Krishnaswamy et al., 2001). Ropelewski and Halpert (1987) identified seventeen global regions with teleconnections between ENSO and regional precipitation, of which Central America and the Caribbean is one. Waylen et

al. (1996) analyzed precipitation totals from over 100 stations in Costa Rica to determine responses of precipitation to ENSO events and found annual precipitation varies by region due to different responses to ENSO. Generally, along Costa Rica's Pacific slope droughts occur during warm (El Niño) events. Specifically, in the Térraba river basin, a hydrologic year may be generally defined as dry (El Niño), wet (La Niña), or normal, depending on the ENSO forcing (Krishnaswamy et al., 2001).

The North Atlantic Oscillation (NAO), a major contributor to interannual variability in atmospheric circulation (Hurrell, 1995), also influences Central American rainfall variability (Giannini et al., 2000; Bhattacharya et al., 2017). The positive phase of the NAO decreases precipitation in the Caribbean region due to surface divergence or subsidence (Giannini et al., 2001). NAO phases also describe the state of the North Atlantic subtropical high (NASH) pressure cell (Lachniet et al., 2017). A positive NAO is associated with a stronger NASH, reducing boundary layer moisture over southern central America (Bhattacharya et al., 2017). Through analysis of proxy and instrumental records and general circulation model simulations, Bhattacharya et al. (2017) found the NAO to be negatively correlated with precipitation in Mexico and Central America, but this correlation is geographically focused along the Atlantic coast. A warm ENSO event paired with a positive NAO phase could constructively interfere to enhance drought conditions, but along the Pacific slope in southern Costa Rica, ENSO is the leading ocean-atmospheric influence on interannual variability (Durán-Quesada et al., 2020).

The latitudinal range of the seasonal migration of the ITCZ also exerts major control over sub-annual and inter-annual patterns of precipitation in Central America and is sensitive to sea surface temperature gradients and radiative forcing between the Northern and Southern Hemispheres (Broccoli et al., 2006). In both the eastern-central Pacific and the Atlantic Oceans

the ITCZ displays an annual cycle of latitudinal migration (Wang and Wang, 1999). Rasmusson and Carpenter (1982) proposed that eastern-central Pacific ITCZ variability is driven by the relationship between sea surface temperature (SST) gradients and ENSO, while the Atlantic ITCZ dynamics are more complex (Chiang et al., 2000).

The Cariaco Basin is located at about 10 °N and represents a well-studied site used to interpret the position of the Atlantic ITCZ through time based on the elemental composition of the laminated marine sediments that accumulate in this marine basin. Haug et al. (2001, 2003) interpreted titanium content (%Ti) in the Cariaco Basin sediments as a direct measure of terrigenous sediment delivery resulting from variations in regional rainfall and river runoff in northern South America. Seasonal patterns of latitudinal migration of the Atlantic ITCZ are recorded in the sediments of the anoxic Cariaco Basin by alternation between terrigenous and marine-dominated material, and the amount of terrigenous material can be used to infer the position of the Atlantic ITCZ (Haug et al., 2001). Generally, a more northerly mean annual position of the Atlantic ITCZ creates wetter conditions for much of the circum-Caribbean and a drier climate is expected when the Atlantic ITCZ is in a more southerly mean annual position (Figure 1, bottom).

2.1.2

Past regional precipitation dynamics

Haug et al. (2003) inferred multiyear drought events through %Ti minima beginning at ca. 1040 cal yr BP, 1090 cal yr BP, 1140 cal yr BP, and 1190 cal yr BP in the Cariaco Basin record. These multiyear drought events coincide with the period known as the Terminal Classic Drought (TCD; 1200 cal yr BP to 850 cal yr BP). The TCD is a period of severe drought that occurred in two distinct phases from about 750–875 AD and ~1000–1075 AD (~1200–1075 cal

yr BP and ~950–875 cal yr BP; Hodell et al., 2005) and is one of the driest intervals in the region within the last millennium (Bhattacharya et al., 2017). Numerous studies have correlated the timing of the TCD to the timing of the demise of the Classic Maya civilization in the Yucatan Peninsula (Haug et al., 2003; Hodell et al., 2005; Webster et al., 2007). Aridity during the TCD is also evident at locales outside of the Yucatan Peninsula including the Basin of Mexico (Lachniet et al., 2012), Caribbean Antilles (Lane et al., 2009b, 2014), Belize (Kennett et al., 2012), Panama (Lachniet et al., 2004), and Costa Rica (Lane and Horn, 2013; Taylor et al., 2013, 2020; Wu et al., 2017, 2019; Kerr, 2019; Kerr et al., 2020).

Several climate forcing mechanisms have been linked to the TCD: changes in solar activity (Hodell et al., 2001), shifts in the ITCZ (Hodell et al., 2005), significant volcanic eruptions in the past 2500 years (Sigl et al., 2015), and anthropogenic deforestation by the Maya and other pre-Columbian peoples (Oglesby et al., 2010). However, Bhattacharya et al. (2017) hypothesized that solar activity changes were quite small over the time period of the TCD. Also, volcanic activity (Sigl et al., 2015) and anthropogenic deforestation (Oglesby et al., 2010; Cook et al., 2012) could have amplified the cooling and aridity of the TCD, but further research is needed to determine if those two mechanisms caused the TCD (Bhattacharya et al., 2017). Bhattacharya et al. (2017) analyzed proxy data and general circulation models to investigate long term drought dynamics in Middle America, which revealed the TCD was driven by basin-wide cooling in the North Atlantic, amplification of the North Atlantic Subtropical High (NASH), and atmospheric drying over southern Central America.

Other notable %Ti minima in the Cariaco Basin record are evident during the timing of the Little Ice Age (LIA) with %Ti levels lower than values occurring during the Younger Dryas (Haug et al., 2001). The LIA is another severe, multidecadal period of drought that may have

253 been a larger magnitude drought than the TCD. Until recently, the LIA was only thought to have
254 affected high-latitude climates, particularly in the North Atlantic. There is now evidence of LIA
255 cooling in the tropical Andes from oxygen isotope compositions of glacial ice (Thompson et al.,
256 2006); sedimentary evidence indicating LIA glacial advance in the Andean highlands (Markgraf
257 et al., 2000; Polissar et al., 2006); geochemical evidence of LIA aridity from sediment cores
258 from the Caribbean slope of the Cordillera Central, Dominican Republic (Lane et al., 2011a), the
259 Yucatan Peninsula (Hodell et al., 2005), Nicaragua (Stansell et al., 2013), and the Gulf of
260 Mexico (Richey et al., 2007); and evidence of LIA cooling from chironomid assemblages in
261 southern Pacific Costa Rica (Wu et al., 2017). Few paleoclimate records include evidence of LIA
262 climate change in the Pacific, but Sachs et al. (2009) documented significant changes in the
263 latitudinal range of migration of the Pacific ITCZ during the LIA. Typically, the modern ITCZ
264 ranges from 3–10 °N in the boreal winter and summer, respectively; however, Sachs et al. (2009)
265 provided evidence of dry climates on Washington Island (4° 43'N, 160° 25' W) in the Northern
266 Line Islands during the LIA related to a near-equator positioned ITCZ, supporting the idea of a
267 change in the latitudinal range of migration of the Pacific ITCZ.

268 The decreased temperatures and increased aridity during the LIA in the high latitudes of
269 the Northern Hemisphere and the circum-Caribbean, respectively, are thought to have been
270 caused by decreases in solar insolation. During the LIA, the Maunder and Spörer sunspot minima
271 occurred (Stuiver and Braziunas, 1989), along with increased volcanic activity (Crowley et al.,
272 2003), resulting in decreased solar insolation that favored a negative NAO phase (Shindell et al.,
273 2001) and weakened the Atlantic Meridional Overturning Circulation (AMOC; Lund et al.,
274 2006). In turn, this decrease in solar insolation caused a decrease in both Atlantic and Caribbean
275 sea surface temperatures (SST; Druffel, 1982; Winter et al., 2000; Wantanabe et al., 2001) and

276 therefore, decreased the cross-equatorial SST gradient. This decreased cross-equatorial SST
277 gradient restricts the ITCZ movement into the northern tropics and results in a drier climate for
278 Central America (Peterson and Haug, 2005; Lane et al., 2011a; Burn and Palmer, 2014).

279 Both the TCD and LIA are hypothesized to have resulted primarily from Atlantic climate
280 variability, leading to droughts in the circum-Caribbean (Lane et al., 2011a; Bhattacharya et al.,
281 2017). Yet, paleorecords used to analyze the TCD (Hodell et al., 1995; 2005; Curtis et al., 1996;
282 Haug et al., 2003; Webster et al., 2007; Lane et al., 2009b, 2011b, 2014; Kennett et al., 2012;
283 Fensterer et al., 2013; Bhattacharya et al., 2015; 2017; Douglas et al., 2015) and the LIA (Haug
284 et al.,2001, 2003; Nyberg et al., 2001; Watanabe et al., 2001; Peterson and Haug, 2005; Lane et
285 al., 2009b, 2011a; Fensterer et al., 2012;) are overwhelmingly located on the Atlantic slope of
286 Middle America and have climate regimes dominated by Atlantic ocean-atmosphere dynamics.
287 To investigate potential Pacific Ocean forcing mechanisms on past precipitation in Central
288 America requires more paleorecords from the Pacific slope. The location of Los Mangos on the
289 Pacific slope in southern Costa Rica and the linkage between ENSO and modern Térraba River
290 Basin streamflow make the site ideal for investigating potential Pacific forcing mechanisms on
291 paleoprecipitation dynamics.

292 *2.1.3*

293 *Existing proxies for Laguna Los Mangos*

294 Sediment in the Los Mangos core varies from fine mineral silts and clays to coarse
295 organic sediment with wood fragments (Johanson et al., 2019). The sediment below the hiatus
296 from ca. 950 to 450 cal yr BP (192–202 cm; Figure 2) shows evidence of incipient pedogenesis
297 on a lake bed exposed by desiccation (Johanson et al., 2019). The hiatus indicates a severe
298 drought that would have affected agricultural activity around Los Mangos (Johanson et al.,

2019). Notably, this does not mean that the drought lasted for 500 years as some sedimentary material may have been lost due to deflation of the exposed lake bed, but does provide bracketing ages for the time period within which the drought occurred.

The Los Mangos pollen record indicates maize agriculture at ca. 3360 cal yr BP. C_3 trees and shrubs, such as Melastomataceae/Combretaceae and *Ficus*, were dominant until the introduction of maize, after which C_3 taxa declined and C_4 grasses and herbs increased (Figure 3). Microscopic charcoal influx is variable at Los Mangos, but shows a slight increase that matches the timing of the first evidence of maize in the record, perhaps related to initial forest clearance (Johanson et al., 2019). Percent organic matter (% OM) increases from less than 10% at the base of the record to ca. 80% at 3100 cal yr BP, and then decreases until the last century (Figure 3; Johanson et al., 2019).

The carbon to nitrogen ratio (C:N) of bulk sediments is sensitive to relative contributions of aquatic vs. terrestrial organic matter inputs to the sedimentary organic matter (SOM) pool. Higher C:N values (>20) indicate that terrestrially-derived organic matter is the dominant contributor to the SOM pool. Lower C:N (<10) indicate aquatic-derived organic matter is the dominant contributor to the SOM pool (Meyers and Ishiwatari, 1993). C:N ratios in Los Mangos are variable, with one large peak at ca. 2900 cal yr BP that indicates an increase in terrestrial carbon deposited in the lake sediments, possibly from deforestation (Figure 3; Kaushal and Binford, 1999; Johanson et al., 2019).

The stable carbon isotopic composition of the bulk sediment ($\delta^{13}C_{TOC}$) toward the base of the Los Mangos core is relatively low (-29.6‰) and remains lower than the profile mean of -27.5‰ until a shift coincident with early maize agriculture at ca. 3360 cal yr BP (Johanson et al., 2019). This shift could represent a transition from primarily C_3 vegetation to increased amounts

of C_4 plants (peak at -24.5‰) associated with maize agriculture. Another relatively positive $\delta^{13}C_{TOC}$ value occurs around the timing of the TCD at ca. 1170 cal yr BP, likely in part due to aridity enhancing water use efficiency in vegetation. Subsequently, $\delta^{13}C_{TOC}$ values decrease by ca. 290 cal yr BP to slightly below mean levels for the record. This decline in $\delta^{13}C_{TOC}$ coincides with the later portion of the LIA (ca. 290 cal yr BP) and the Spanish Conquest (ca. 450 cal yr BP). The most recent section of the core shows increasing $\delta^{13}C_{TOC}$ values that are indicative of modern agriculture. However, the $\delta^{13}C_{TOC}$ record is influenced by both changes in plant species assemblages (C_3 vs C_4 vegetation) and water use efficiency (Diefendorf and Freimuth, 2017), thus, adding $\delta^{13}C_{C29}$ and $\delta^{13}C_{C31}$ records will help disentangle variability within the $\delta^{13}C_{TOC}$ record.

3.0 Materials and methods

3.1 n-alkane extraction

Following the methods of Lane et al. (2018) for extraction and purification of *n*-alkanes, we lyophilized 61 sediment samples and ground them to a homogenized powder using a mortar and pestle. We used an accelerated solvent extractor, ASE 350 Dionex California, U.S.A. system, with hexane at 125°C at a pressure of 1500 psi for 10 minutes to solvent-extract *n*-alkanes. The excess solvent added during the ASE process was removed using a rotary evaporator to condense the *n*-alkanes in each sample. To isolate the aliphatic fraction of the solvent extracted *n*-alkanes, we used silica column chromatography solid phase extraction with

hexane as the eluting solvent. Lastly, we conducted urea adduction to isolate straight-chain monomers from branched and cyclic compounds within the aliphatic fraction.

3.1.1

Identification and quantification

We identified and quantified *n*-alkane abundances using a Thermo 1310 gas chromatograph coupled with an ISQ quadrupole mass spectrometer and a flame ionization detector. To confirm identification and quantify abundance, a standard of C_7-C_{40} *n*-alkane mixture (Sigma Aldrich) was used in full scan mode and compared to all sample spectra. A TG-5 SILMS silica column (30m, 0.32mm i.d., 0.32µm film thickness) was used with an oven temperature program of 70°C isothermal for 1 minute, 20°C/min to 180°C, 4°C/min to 320°C, 320°C isothermal for 5 minutes, 30°C/min to 350°C, and 350°C isothermal for 1 minute for the gas chromatograph injections completed in splitless mode at 300°C. The abundances of *n*-alkanes are presented in units of µg g OM^{-1}, where OM is the percent organic matter as determined by loss on ignition analyses by Johanson et al. (2019). We used the average chain length (ACL) equation of Diefendorf et al. (2011) and the carbon preference indices (CPI) equation proposed by Marzi et al. (1993) to determine the dominant carbon source.

3.1.2

Compound-specific stable isotope analyses

We conducted compound-specific carbon and hydrogen isotope ratio analyses of *n*-alkanes using a Thermo Delta V plus mass spectrometer coupled with a Thermo 1310 gas chromatograph via an Isolink II device. We used a Thermo TG-5 SILMS silica column (60m, 0.25mm i.d., 0.25µm film thickness) for homologue separation. The injection and oven temperature parameters were the same as the programs used for the identification and

quantification of compounds. We injected Indiana University mixture B4 as alkane standards every third sample to monitor sample precision. We analyzed samples in duplicate and precision was calculated based on multiple injections of a single alkane sample. We corrected raw data to the Vienna Pee-Dee Belemnite (for $\delta^{13}C$ data) and Vienna Standard Mean Ocean Water (for $\delta^{2}H$ data) standards using the Indiana University mixture B4 standard. The standard error for all sample measurements was calculated using the methods of Polissar and D'Andrea (2014).

3.1.3

Apparent fractionation (ε) corrections

Feakins (2013) paired hydrogen isotope values for plant leaf wax ($\delta^{2}H_{wax}$) with pollen data from the same sediments to evaluate species-specific isotopic fractionation and devise a way to correct for potential bias in paleohydrological reconstructions from $\delta^{2}H_{wax.}$. We used a modified version of Feakins' (2013) end-member mixing model to correct the $\delta^{2}H$ composition of each individual C_{29} and C_{31} alkane sample for variations in apparent isotope fractionation (ε) between precipitation and leaf waxes based on co-occurring or stratigraphically adjacent fossil pollen assemblages. We present hydrogen isotopic values only from alkanes C_{29} and C_{31} as we are interested in changes in the terrestrial climate and higher chain length *n*-alkanes are derived from terrestrial higher plants (Eglinton and Hamilton, 1967). We grouped existing pollen counts from Los Mangos into appropriate plant life form categories to determine the approximate contribution of each plant life form to the total pollen sum. The isotopic end-members were determined using data provided by Sachse et al. (2012) for ε of C_{29} and C_{31} alkanes by plant life form, as angiosperms, C_3 graminoids, C_4 graminoids, forbs, and pteridophytes have different ε values (Appendix, Table A.1). Gymnosperm ε values were omitted from the mixing model calculations because there are no gymnosperms in the study area. The same technique used by

Kerr (2019) was applied to correct the hydrogen isotope values for alkanes C_{29} and C_{31} (C_x) using estimated ε values from pollen counts. The ε values were calculated as:

$$\varepsilon C_x = [\, f C_{3\ \text{Angiosperm trees and shrubs}} * \varepsilon C_{3\ \text{Angiosperm trees and shrubs}}] + [\, f C_{3+C4\ \text{Graminoids}} * \%C_3\ \text{Graminoids} * \varepsilon C_{3\ \text{Graminoids}}] + [\, f C_{3+C4\ \text{Graminoids}} * \%C_4\ \text{Graminoids} * \varepsilon C_{4\ \text{Graminoids}}] + [\, f C_{3+C4\ \text{Forbs}} * \varepsilon C_{3+C4\ \text{Forbs}}] + [\, f_{\text{Pteridophytes}} * \varepsilon_{\text{Pteridophytes}}]$$

Where the fraction of pollen by type (f_x) is derived from the values calculated by grouping Los Mangos pollen data by plant life form and ε is equal to the apparent fractionation values for C_{29} and C_{31} by growth form provided by Sachse et al. (2012).

The ε-corrected hydrogen isotope (ε-corrected δ^2H) values for the alkanes C_{29}, and C_{31} (C_x) are calculated for each individual sample as:

$$\varepsilon\text{–corrected } \delta^2H_{C29,31} = ((\delta^2H_{(Cx)} + 1000)/((\varepsilon_{Cx}/1000)+1))-1000$$

Where δ^2H_{Cx} is equal to the raw δ^2H values of C_{29}, and C_{31} found for each Los Mangos sample and ε_{Cx} is equal to the calculated ε for C_{29} and C_{31} based on the co-occurring or stratigraphically adjacent pollen assemblage for each sample (Figure 4 and Appendix, Table A.2).

4.0

Results

The CPI of alkanes in the Los Mangos samples range from 0.861 to 7.01 with an average of 3.28. The ACL of alkanes in all samples is 23.3. The most abundant *n*-alkane in each sample is C_{29}. The average $\delta^{13}C$ values of C_{29} and C_{31} *n*-alkanes ($\delta^{13}C_{C29}$ and $\delta^{13}C_{C31}$) for the entire Los Mangos record are -33.3‰ and -34.0‰, respectively (Figure 5, Appendix, Table A.2). The $\delta^{13}C_{C29}$ and $\delta^{13}C_{C31}$ values are variable before the largest positive excursion at 3071 cal yr BP

412 with a $\delta^{13}C_{C29}$ value of -30.1‰ and a $\delta^{13}C_{C31}$ value of -28.9‰. The $\delta^{13}C_{C29}$ and $\delta^{13}C_{C31}$ values
413 show a sharp positive increase at 1713 cal yr BP to -31.5‰ and -30.9‰, respectively. The
414 beginning of the Terminal Classic Drought (TCD), before the hiatus, displays a slight increase in
415 $\delta^{13}C_{C29}$ and $\delta^{13}C_{C31}$ values. The early LIA has more negative $\delta^{13}C_{C29}$ and $\delta^{13}C_{C31}$ values that are
416 slightly below the average $\delta^{13}C_{C29}$ and $\delta^{13}C_{C31}$ values for the entire record. At 285 cal yr BP,
417 corresponding to the middle LIA, the $\delta^{13}C_{C29}$ value of -32.8‰ is above the entire record average
418 $\delta^{13}C_{C29}$ value, but following this there is a trend toward more negative $\delta^{13}C_{C29}$ values at the top of
419 the sedimentary record. The carbon isotopic composition of C_{29} *n*-alkanes is not strongly
420 correlated with the carbon isotopic composition of the bulk sediment ($R^2 = 0.205$) but the
421 relationship is statistically significant ($p = 4.01$ E-17, n=23).
422 The average ε-corrected $\delta^{2}H_{C29}$ (Figure 4) and $\delta^{2}H_{C31}$ (Appendix, Table A.2) values of
423 the Los Mangos sedimentary record are -57.3‰ and -56.1‰, respectively, and isotopically
424 lighter than the modern precipitation $\delta^{2}H$ value of -47.0‰ estimated for Los Mangos (Bowen,
425 2019). The $\delta^{2}H_{C29}$ and $\delta^{2}H_{C31}$ profiles closely resemble the $\delta^{13}C_{C29}$ and $\delta^{13}C_{C31}$ profiles until ca.
426 3360 cal yr BP. Following ca. 3360 cal yr BP, the most negative hydrogen isotope values occur
427 at 3071 cal yr BP ($\delta^{2}H_{C29}$ = -122‰; $\delta^{2}H_{C31}$ = -96.6‰), corresponding with the most positive
428 $\delta^{13}C_{C29}$ and $\delta^{13}C_{C31}$ values. The $\delta^{2}H_{C29}$ and $\delta^{2}H_{C31}$ values then become variable with a 100-year
429 period of aridity lasting from approximately 1850–1750 cal yr BP as indicated by above-average
430 $\delta^{2}H_{C29}$ and $\delta^{2}H_{C31}$ values. The early TCD has slightly above-average $\delta^{2}H_{C29}$ and $\delta^{2}H_{C31}$ values at
431 1198 cal yr BP ($\delta^{2}H_{C29}$ = -51.0‰; $\delta^{2}H_{C31}$ = -50.1‰) before transitioning to below-average $\delta^{2}H$
432 values at 1166 cal yr BP. The early LIA reveals a sharp positive $\delta^{2}H_{C29}$ peak at 397 cal yr BP
433 with a $\delta^{2}H_{C29}$ value of -32.0‰. The middle LIA $\delta^{2}H_{C29}$ and $\delta^{2}H_{C31}$ values remain slightly above
434 the average $\delta^{2}H_{C29}$ and $\delta^{2}H_{C31}$ values for the record until 285 cal yr BP. After 285 cal yr BP, the

late LIA and modern (100 cal yr BP to present) δ^2H_{C29} and δ^2H_{C31} values remain below the average δ^2H_{C29} and δ^2H_{C31} for the record.

5.0 Discussion

Out of the three sediment cores taken within the western portion of the Diquís subregion, the Los Mangos record begins well before the Lagunas Danta and Carse records. The 4200 cal yr BP record of Los Mangos contains an 840 cal yr period prior to the first evidence of maize pollen in the record. This period is representative of the pre-agricultural landscape surrounding Los Mangos, which was dominated by C_3 vegetation before 3360 cal yr BP (Johanson et al., 2019). Both C_3 and C_4 species have a range of $\delta^{13}C$ values due to environmental and biological factors (Diefendorf and Freimuth, 2017) and enzymatic subtypes (Hattersley, 1982). Various environmental factors influence the $\delta^{13}C$ signatures of C_3 plants, generating a larger range of $\delta^{13}C$ values as compared to those of C_4 species, 20‰ vs 10‰, respectively. Climate generates large net isotope effects on C_3 plants through the influence of precipitation on stomatal conductance (Farquhar et al., 1989; Diefendorf and Freimuth, 2017). Decreased precipitation reduces stomatal conductance and increases water use efficiency in plants, which would increase the $\delta^{13}C_{C29}$ and $\delta^{13}C_{C31}$ values of alkanes (Farquhar et al., 1989; Diefendorf and Freimuth, 2017).

The 10‰ difference between ε-corrected (this study) and the modern precipitation δ^2H values may be due to small changes in the fractional contributions of different plant life forms throughout the 4200 cal yr BP sedimentary record of Los Mangos or the seasonal timing of alkane biosynthesis, which most likely occurs during the wet season when precipitation δ^2H values are lower (Sánchez-Murillo et al., 2016). The δ^2H values of terrestrially-derived *n*-alkanes

458 are controlled by a combination of the δ^2H composition of precipitation, subsequent
459 evapotranspiration of soil water prior to plant uptake, and species-specific biosynthetic
460 fractionations during lipid biosynthesis (Sachse et al., 2012). The δ^2H of precipitation in tropical
461 locales is typically assumed to be controlled primarily by the δ^2H of atmospheric vapor source
462 waters and subsequent rainout, otherwise known as the 'amount effect', with higher rates of
463 precipitation corresponding to lower δ^2H values of precipitation (Sachse et al., 2012). However,
464 Sánchez-Murillo et al. (2016) proposed that the amount effect is not a significant control on
465 precipitation δ^2H values and that moisture source (Pacific vs. Atlantic) has minimal influence on
466 southern Costa Rican regional precipitation δ^2H values. Sánchez-Murillo et al. (2016)
467 documented large decreases in precipitation δ^2H values during the wet season (65‰) as
468 compared to the dry season (19‰) that show strong statistical relationships with relative
469 humidity and lifting condensation level, which are themselves interrelated. The data of Sánchez-
470 Murillo et al. (2016) indicate that not only are precipitation δ^2H values a strong proxy for mesic
471 vs. arid conditions, but also that moisture source and transport are not the primary controls on
472 regional δ^2H values. If moisture source or transport were the primary drivers of precipitation
473 δ^2H values in the region, the expected pattern would be more negative precipitation δ^2H values
474 during the dry season due to the combined effects of Atlantic-sourced moisture that has a lower
475 δ^2H value than that of the Pacific, and subsequent orographic distillation of air masses moving
476 over the Cordillera.

477 Based on these modern dynamics and isotopic systematics, we interpret a decrease in
478 δ^2H_{alkane} values to indicate an increase in relative humidity and overall precipitation while
479 increased δ^2H_{alkane} values indicate decreased relative humidity and decreased overall
480 precipitation. For instance, at 4053 cal yr BP a relatively low δ^2H_{C29} value (-74.3‰), in

comparison to the record average, indicates an increase in relative humidity and overall precipitation. At 3907 cal yr BP δ^2H_{C29} values increase and remain above the record average for about 200 years, signaling a period of decreased relative humidity and decreased overall precipitation (Figure 4).

A slight increase in $\delta^{13}C_{C29}$ and $\delta^{13}C_{C31}$ values after the first occurrence of maize pollen at 3360 cal yr BP likely indicates a small increase in the contribution of C_4 plants to the sedimentary organic pool, associated with land clearance and the establishment of C_4 crops and associated weeds. After 3360 cal yr BP the δ^2H_{C29} and δ^2H_{C31} values shift toward more negative values as compared to the record averages, which we interpret as an increase in relative humidity and overall precipitation. Also, during this time $\delta^{13}C_{TOC,}$ C/N, % OM, and P/Al values slightly increase and maize pollen is present, supporting the interpretation of active agriculture and land modification around Los Mangos (Figure 5). Thus, the slight increase in both $\delta^{13}C_{C29}$ and $\delta^{13}C_{C31}$ values after the first occurrence of maize pollen at 3360 cal yr BP most likely reflect organic matter contributions from vegetation composed of different plant species, such as an increase in C_4 crops and weeds, as opposed to reflecting increased water use efficiency due to limited precipitation. The small amplitude of the positive excursion, <1‰, indicates that cultivation may have been on a relatively small scale during the earliest stages of site occupation. Further, the relatively small differences (<4‰) in $\delta^{13}C_{C29}$ values between intervals of maize agriculture and later forest regeneration at Los Mangos indicate less replacement of C_3 vegetation (e.g., tropical forest) by cultigens or associated weedy taxa at Los Mangos compared to Laguna Santa Elena (~8‰ compound-specific isotopic data; Kerr, 2019), located ca. 65 km to the southeast. Proxy evidence of relatively low C_4 biomass at Mangos could represent smaller scale agricultural

503 activities or a greater reliance on C_3 cultigens relative to these other sites in the southern Pacific
504 region.

505 The similar trends in the $\delta^{13}C_{TOC}$ record (Johanson et al., 2019) and the $\delta^{13}C_{C29}$ record
506 (this study) may signify that both proxies are responding similarly to temporal changes in
507 vegetation around Los Mangos (Lane et al., 2016) prior to ca. 3360 cal yr BP. The relationship
508 between the proxies is not strongly correlated ($R^2 = 0.205$), but is statistically significant ($p =$
509 4.01 E-17, $n = 23$). This result is likely the consequence of data points that deviate from the
510 linear regression, which most likely reflects the sensitivity of $\delta^{13}C_{TOC}$ values to different carbon
511 sources (Meyers and Ishiwatari, 1993). In contrast, $\delta^{13}C_{C29}$ values reflect sedimentary plant
512 waxes (Diefendorf and Freimuth, 2017) and may better quantify proportional contributions of C_3
513 vs. C_4 vegetation to the landscape (Goldsmith et al., 2019). Lane et al. (2016) compared coeval
514 $\delta^{13}C_{C29}$ and $\delta^{13}C_{TOC}$ values from Laguna Castilla, Dominican Republic and found them to be
515 positively correlated ($R^2 = 0.52$). The authors interpreted this matched temporal response of the
516 $\delta^{13}C_{C29}$ and $\delta^{13}C_{TOC}$ proxies to indicate a lack of 'pre-aging' of alkanes in the terrestrial
517 environment before burial in the lake sediments (Lane et al., 2016). However, the lack of a
518 strong correlation between $\delta^{13}C_{C29}$ and $\delta^{13}C_{TOC}$ values in the Los Mangos record does not
519 necessarily indicate an age offset exists or that the proxies are not responding temporally to shifts
520 in vegetation, because bulk sedimentary isotope proxies represent organic matter from different
521 sources (Lane et al., 2016). Instead, the lack of a strong temporal correlation between the $\delta^{13}C_{TOC}$
522 and $\delta^{13}C_{C29}$ records for the Los Mangos proxies is likely because both nonvascular aquatic plants
523 (C:N = 4–10) and vascular land plants (C:N = ≥20) (Meyers and Ishiwatari, 1993) have
524 contributed to the sedimentary organic matter pool. Mean C:N ratios of 13.6 in the Los Mangos

record indicate a well-mixed sedimentary organic matter pool of both allochthonous and autochthonous origin.

At 3071 cal yr BP the $\delta^{13}C_{C29}$ and $\delta^{13}C_{C31}$ values reach the highest levels for the entire record, which could be interpreted as an increase in C_4 vegetation and/or drought stress. This increase corresponds to the most negative δ^2H_{C29} and δ^2H_{C31} values in the entire Los Mangos record, the highest C:N ratio, highest concentration of organic matter, a slight increase in charcoal influx, a shift in elemental composition of the sediments (P/Al), and the presence of maize pollen (Figure 5). As previously mentioned, more negative δ^2H_{C29} and δ^2H_{C31} values indicate increased relative humidity and increased overall precipitation, but Rosenmeier et al. (2002) proposed the hypothesis that extensive deforestation could significantly alter hydrological budgets of lake basins, thereby causing the δ^2H_{alkane} proxies to reflect hydrologic change due to land use instead of precipitation variability. Inferred land use change around Los Mangos at ca. 3071 cal yr BP may have influenced the δ^2H_{C29} and δ^2H_{C31} records as deforestation reduces the rates of transpiration at the basin scale and, as a result of decreased soil moisture flux, can theoretically reduce the δ^2H value of groundwater (Rosenmeier et al., 2002) used by plants during lipid biosynthesis.

The most positive δ^2H_{C29} and δ^2H_{C31} values of the entire Los Mangos record occur at ~1840 cal yr BP and are preceded by ~200 years of variable δ^2H values. This period of inferred hydrologic variability terminated by extended drought appears to have potentially affected agriculture around Los Mangos as indicated by a 250-year hiatus in maize pollen deposition and lack of evidence of site occupation in other proxy data, for example low charcoal area influx (Figure 5).

Johanson et al. (2019) concluded that drought in the lowlands of southern Pacific Costa Rica during the late Terminal Classic Drought (TCD) was a driver of the sediment hiatus that began after 950 cal yr BP in the Los Mangos record. Several sites in Costa Rica and the wider circum-Caribbean contain evidence of increased aridity during the TCD: Laguna Zoncho (Wu et al., 2017; Taylor et al., 2020), Lago de las Morrenas 1 (Kerr, 2019), Lago de las Morrenas 3C (Wu et al., 2019), Laguna Bonillita (Kerr, 2019), and Las Lagunas (Lane et al., 2009b, 2014). However, these sites with evidence of TCD aridity, with the exception of Laguna Zoncho (65 km southeast of Los Mangos), are all in Atlantic watersheds. Kerr (2019) concluded that Laguna Santa Elena, located near Laguna Zoncho, was not consistently dry during the TCD, but had variable precipitation conditions. Warm ENSO events should result in drought around Los Mangos based on the positive correlation between regional precipitation and ENSO (Krishnaswamy et al., 2001). Thus, amplified ENSO event frequency coinciding with the TCD should include warm events that may be responsible for the documented desiccation of Los Mangos, which is in contrast to the hypothesis that climate variability in the Atlantic was the primary mechanism forcing circum-Caribbean droughts around this time period (Bhattacharya et al., 2017). While amplified ENSO events should also include wet periods for Los Mangos, our record does show slightly below average δ^2H_{C29} and δ^2H_{C31} values at 1166 cal yr BP that coincide with maize pollen presence just before the sedimentary hiatus, which could represent wetter conditions prior to an extreme dying event. Lachniet et al. (2004) also documented dry conditions in eastern Panama, ~30 km from the Pacific coast, during this period and concluded ENSO is the primary driver of precipitation anomalies for the study region and possibly the entire Pacific coast of Central America.

569 Warm ENSO events are associated with increases in northeast trade wind and Caribbean
570 Low-Level Jet velocities (Hastenrath and Lamb, 1977) and as these winds reach Costa Rica the
571 rain shadow is enhanced along the Pacific slope of the cordilleras (Vargas and Trejos, 1994).
572 Typically, the northerly migration of the ITCZ in the boreal summer perturbs the rain shadow,
573 bringing precipitation to the Pacific slope of Costa Rica (Waylen et al., 1996), but a decreased
574 cross-equatorial SST gradient would inhibit northward movement of the ITCZ, a consequence of
575 an El Niño event (Figure 1, bottom). Proxy records of El Niño events from Laguna Pallcacocha,
576 Ecuador (Moy et al., 2002) reveal maximum ENSO frequency during the TCD. While the
577 Laguna Pallcacocha ENSO proxy record has received some criticism for potentially not
578 capturing all ENSO events accurately (Schneider et al., 2018), other sites throughout the Pacific
579 support the hypothesis of enhanced El Niño frequency and strength coincident with the TCD.
580 The El Junco Lake, Galapagos record (Conroy et al., 2008) contains grain size evidence of
581 enhanced El Niño frequencies between ~1000 and 500 cal yr B.P. relative to the preceding 500
582 years. Sedimentary records from the Western Pacific also indicate increased amplitude of ENSO
583 events during the TCD (Rodysill et al., 2019). Sachs et al. (2021) found evidence of drying in
584 δ^2H records from Washington Island, but concluded that this drying is likely from large volcanic
585 eruptions because the apparent increase in El Niño frequency during this time should have led to
586 greater precipitation on Washington Island. We propose that lake desiccation, decreased
587 agricultural proxies, and increases in $\delta^{13}C_{C29}$ and $\delta^{13}C_{C31}$ values during the TCD at Los Mangos
588 resulted largely from Pacific climate forcing mechanisms, such as high-amplitude or high-
589 frequency El Niño events. Koutavas et al. (2006) found variance in Pacific-based $\delta^{18}O$ data from
590 *G. ruber* foraminifera to be strongly correlated to ENSO dynamics during the late Holocene,
591 while mid-Holocene $\delta^{18}O$ data showed no correlation with ENSO. George et al. (1998) analyzed

592 modern stream flow data and found that Costa Rican watersheds draining into the Pacific had
593 strong connections to ENSO cyclicity whereas rivers draining into the Caribbean showed unclear
594 connections to ENSO cyclicity. Thus, both past (Koutavas et al., 2006) and modern (George et
595 al., 1998) Pacific records show a strong connection to ENSO cyclicity and strength. The drying
596 observed at Los Mangos during the TCD is likely due to this locale being heavily influenced by
597 increased El Niño frequency or strength at this time.

598 The Little Ice Age (LIA) also appears to have affected precipitation dynamics around Los
599 Mangos, but at an apparently lower evaporation to precipitation ratio as compared to the TCD
600 because the Los Mangos record does not include evidence of lake desiccation during the LIA.
601 The Los Mangos δ^2H_{C29} profile indicates a wet early LIA (453 to 434 cal yr BP), dry middle LIA
602 (434 to ca. 300 cal yr BP), and wet late LIA (ca. 300 to present). In contrast, the sediments of the
603 Cariaco Basin display the lowest %Ti values of the entire Holocene during the middle LIA. At
604 this time, Los Mangos δ^2H_{C29} and δ^2H_{C31} proxies signal drier than average conditions, but there is
605 no evidence of lake desiccation like that observed for the TCD. After ca. 300 cal yr BP both the
606 δ^2H_{C29} and δ^2H_{C31} proxies and the Cariaco Basin %Ti profile show increases in precipitation with
607 below-average δ^2H_{C29} and δ^2H_{C31} values and higher Ti percentages, respectively (Figure 6). Also,
608 in Pacific Costa Rica, Kerr (2019) documented increased δ^2H_{alkane} values around 215 cal yr BP at
609 Santa Elena and interpreted the increased δ^2H_{alkane} values as evidence of severe drying towards
610 the end of the LIA. Los Mangos δ^2H_{C29} and δ^2H_{C31} values increased starting ca. 430 cal yr BP and
611 the apparent drying persisted for about 130 years before transitioning to wetter than average
612 moisture conditions as the LIA ended (Figure 6). The period of aridity at Santa Elena lasted
613 longer, for a total of 330 cal yr, until the end of the LIA (Kerr, 2019). The lack of evidence of
614 severe drought during the LIA, such as expressed by the unconformity during the TCD, may

615 implicate Atlantic basin climate dynamics as the primary forcing mechanism of arid conditions
616 during the LIA. Lane et al. (2011a) summarized widespread proxy evidence of LIA paleoclimate
617 and palaeoceanographic change in the western tropical Atlantic that is consistent with a decrease
618 in the Atlantic meridional overturning circulation (AMOC) that would drive a decrease in
619 Caribbean SSTs and a diminished cross-equatorial SST gradient, leading to a southward
620 suppression of the ITCZ.

621 Analyzing total lipid extract (TLE) δ^2H values from a sediment core containing a
622 microbial mat, Sachs et al. (2009) found that Washington Lake (4° 43'N, 160° 25' W) on
623 Washington Island, part of the Northern Line Islands in the central Pacific Ocean, also
624 experienced extended periods of decreased precipitation from ca. 530 to 390/310 cal yr BP and
625 periods of increased precipitation after 390–310 cal yr BP. Presently, Washington Island receives
626 about 2900 mm of precipitation per year due to its position within the latitudinal range of the
627 annual migration of the Pacific ITCZ (Sachs et al., 2009). The sedimentary record of Washington
628 Lake indicates the most arid conditions relative to the entire record occurred during the LIA (530
629 to 390–310 cal yr BP) based on positive hydrogen isotope values of total lipid extracts, inferred
630 high salinity, and a gelatinous red-orange microbial mat containing the extremely salt-tolerant
631 cyanobacteria, *Aphanothece* (Sachs et al., 2009). Sachs et al. (2009) concluded the mean annual
632 position of the Pacific ITCZ was located south of Washington Island during a portion of the LIA,
633 creating hypersaline conditions in Washington Lake, but this southward positioning of the
634 Pacific ITCZ was short lived. The most arid conditions on Washington Island, 530–390/310 cal
635 yr BP, correlate to arid conditions at Los Mangos, ca. 430–300 cal yr BP. After 300 cal yr BP,
636 Los Mangos transitioned to a wetter climate with two significant periods of increased
637 precipitation indicated by negative δ^2H_{C29} and δ^2H_{C31} values at 285 and 130 cal yr BP.

638 Sachs et al. (2009) also documented δ^2H values from dinosterol, a lipid from
639 dinoflagellate algae, signaling a transition to a wetter climate in Spooky Lake, Palau (7°09'N,
640 134° 22'E), and δ^2H values from botryococcenes, a lipid from the B race of green algae, in El
641 Junco Lake, Galápagos (0° 54' S, 89° 29' W) signaling a transition to a drier climate after
642 approximately 150 cal yr BP (Figure 6). The increased $\delta^2H_{botryococcenes}$ values from El Junco Lake
643 after 150 cal yr BP temporally correlate to decreased δ^2H_{lipid} values from Los Mangos,
644 Washington Lake, and Spooky Lake, which is expected due to the position of each study site.
645 Los Mangos, Washington Lake, and Spooky Lake all lie near or just north of the northern extent
646 of the modern annual position of the Pacific ITCZ while El Junco Lake lies south of it. Thus,
647 opposing δ^2H records from Los Mangos, Washington Lake, and Spooky Lake compared to El
648 Junco Lake support the idea that the near-equator positioned Pacific ITCZ eventually migrated
649 northward, producing a wetter climate at Los Mangos, Washington Lake, and Spooky Lake
650 toward the late-LIA (Sachs et al., 2009).
651 Cooling in the Northern Hemisphere during the LIA most likely decreased the cross-
652 equatorial sea surface temperature gradient, keeping the Pacific ITCZ further south (Sachs et al.,
653 2009) and creating drier conditions at Los Mangos. Rodysill et al. (2019) proposed that La Niña
654 related flooding in Indonesia decreased at the end of the Medieval Climate Anomaly (MCA) and
655 the early LIA due to decreased amplitudes (rainfall extremes) of ENSO events during this period
656 of relatively cool Northern Hemisphere temperatures. Rodysill et al. (2019) suggested ENSO-
657 driven precipitation dynamics become more extreme during periods of above average Northern
658 Hemisphere mean temperatures. The TCD overlaps with the Medieval Warm Period, a time
659 period known for warmer than average Northern Hemisphere temperatures. Desiccation of Los
660 Mangos sediments during the TCD may have occurred due to more severe (higher amplitude

661 increases in evaporation to precipitation ratios) warm-phase ENSO-driven droughts during this
662 relatively warm period of the late Holocene. Conversely, the LIA may have been a period of
663 lower-amplitude (smaller amplitude increases in evaporation to precipitation ratios) droughts that
664 never led to desiccation of the Los Mangos lake basin. This conceptual model implicates both
665 Pacific (ENSO) and Atlantic (NAO/NASH) dynamics as potential drivers of drought conditions
666 in the circum-Caribbean over the last 2000 years, with particularly arid conditions possibly
667 related to high-amplitude warm phases of ENSO, perhaps in concert with an expanded NASH.
668
669 6.0
670 Conclusions
671 Sedimentary and radiocarbon evidence of a hiatus in sedimentation signifies extreme
672 drought during the TCD at Los Mangos. Conversely, the *n*-alkane hydrogen isotope proxies
673 (δ^2H_{wax}; Figure 6 and Appendix, Table A.2) at Los Mangos indicate relatively small decreases in
674 precipitation during the LIA. We propose that ocean-atmosphere dynamics of both Atlantic and
675 Pacific basins influenced drought events at Los Mangos. However, drought impacts at Los
676 Mangos during the TCD were apparently much more severe than during the LIA. This contrast in
677 drought amplitude is in good agreement with recent and past records of ENSO-driven rainfall
678 extremes in the Pacific basin, indicating that TCD and LIA drought dynamics in the neotropics
679 were not solely controlled by North Atlantic ocean-atmosphere dynamics. The TCD, in
680 particular, may have been related primarily to Pacific ocean-atmosphere dynamics (ENSO) and
681 resulting teleconnections, in contrast to the LIA, for which Atlantic expressions of the climatic
682 event appear to be more severe.

Author contributions

Lane, Horn, Johanson, and Gamble designed the research and Horn and Johanson collected the sediment core used for analyses. Lane and Yanuskiewicz conducted compound-specific isotope analyses of the Laguna Los Mangos sediment samples and wrote the majority of the manuscript. Johanson contributed pollen, charcoal, and bulk sediment geochemistry data, significantly contributing to the manuscript; assisted with figure development; and provided manuscript edits. Horn contributed pollen data expertise and significantly edited the manuscript.

Data availability

All data are available by request to the authors.

Declaration of competing interest

The authors declare that they have no known competing financial interests or personal relationships that could have appeared to influence the work reported in this paper.

Acknowledgements

We thank Krysden Schantz for assistance with isotope sample processing, and Kimberly Duernberger for assistance with isotopic measurements. We also thank Matthew Kerr for assistance with isotopic measurements and guidance in the correction of raw isotopic values.

Funding

This research was funded by the National Science Foundation (Award #1660185) and the UNCW College of Arts and Sciences.

706 7.0

707 References

708 Anchukaitis K.J., and Horn, S.P., 2005. A 2000-year reconstruction of forest disturbance from
709 southern Pacific Costa Rica. Palaeogeography, Palaeoclimatology, Palaeoecology 221,
710 35–54.
711
712 Berger, A., and Loutre, M.F., 1991. Insolation values for the climate of the last 10 million years.
713 Quaternary Science Reviews, 10, 297–317.
714
715 Bhattacharya, T., Byrne, R., Böhnel, H., Wogau, K., Kienel, U., Ingram, B.L., Zimmerman, S.,
716 2015. Cultural implications of late Holocene climate change in Cuenca Oriental, Mexico.
717 Proceedings of the National Academy of Sciences, 112, 1693–1698.
718
719 Bhattacharya, T., Chiang, J.C.H., Cheng, W., 2017. Ocean-atmosphere dynamics linked to
720 8001050 CE drying in Mesoamerica. Quaternary Science Reviews, 169, 263–277.
721
722 Bowen, G. J., 2019. The Online Isotopes in Precipitation Calculator, version 3.1.
723 http://www.waterisotopes.org.
724
725 Broccoli, A.J., 2006. Response of the ITCZ to Northern Hemisphere cooling. Geophysical
726 Research Letters, 33, 1–4.
727
728 Burn, M.J., Palmer, S.E., 2014. Solar forcing of Caribbean drought events during the last
729 millennium. Journal of Quaternary Science, 29, 827–836.
730
731 Chiang, J.C.H., Kushnir, Y., Zebiak, S.E., 2000. Interdecadal changes in eastern Pacific ITCZ
732 variability and its influence on the Atlantic ITCZ. Geophysical Research Letters, 27,
733 3687–3690.
734
735 Clement, R.M., and Horn, S.P., 2001. Pre-Columbian land-use history in Costa Rica: a 3000-year
736 record of forest clearance, agriculture and fires from Laguna Zoncho. The Holocene,
737 11,4, 419–426.
738
739 Conroy, J.L., Overpeck, J.T., Cole, J.E., Shanahan, T.M., Steinitz-Kannan, M., 2008. Holocene
740 changes in eastern tropical Pacific climate inferred from a Galápagos lake sediment
741 record. Quaternary Science Reviews, 27, 1166–1180.
742
743 Cook, B., Anchukaitis, K., Kaplan, J., Puma, M., Kelley, M., Gueyffier, D., 2012. Pre-
744 Columbian deforestation as an amplifier of drought in Mesoamerica. Geophysical
745 Research Letters, 39, 1–5.
746
747 Corrales F (2000) An Evaluation of Long Term Cultural Change in Southern Central America.
748 University of Kansas (Dissertation), 1–361.
749

Covey, D. L., and S. Hastenrath, 1978: Pacific El Niño phenomenon and the Atlantic circulation. Monthly Weather Review, 106, 1280–1287.

Crowley, T.J., Baum, S.K., Kim, K.Y., Hegerl, G.C., Hyde, W.T., 2003. Modeling ocean heat content changes during the last millennium. Geophysical Research Letters, 30, 1–4.

Curtis, J.H., and Hodell, D.A., 1996. Climate variability on the Yucatan Peninsula (Mexico)during the past 3500 years, and implications for Maya culture evolution. Quaternary Research, 46, 37–47.

Curtis, S., and Hastenrath, S., 1995: Forcing of anomalous sea surface temperature evolution in the tropical Atlantic during Pacific warm events. Journal of Geophysical Research, 100, 15,835–15,847.

Diefendorf, A.F., Freeman, K.H., Wing, S.L., Graham, H.V., 2011. Production of n-alkyl lipids in living plants and implications for the geologic past. Geochimica et Cosmochimica Acta, 75, 7472–7485.

Diefendorf, A.F., and Freimuth, E.J., 2017. Extracting the most from terrestrial plant derived nalkyl lipids and their carbon isotopes from the sedimentary record: A review. Organic Geochemistry 103, 1–21.

Dobyns, H.F., 1966. An appraisal of techniques with a new hemispheric estimate. Current Anthropology 7: 395–416.

Douglas, P.M.J., Pagani, M., Canuto, M.A., Brenner, M., Hodell, D.A., Eglinton, T.I., Curtis,J.H., 2015. Drought, agriculture adaptation, and sociopolitical collapse in the Maya Lowlands. Proceedings of the National Academy of Sciences, 112, 5607–5612.

Druffel, E.M., 1982. Banded corals: Changes in oceanic carbon-14 during the Little Ice Age. Science, 218, 13–19.

Durán-Quesada, A.M., Sorí, R., Ordoñez, P., Gimeno, L., 2020. Climate perspectives in the Intra-Americas Seas. Atmosphere, 11, 959; doi:10.3390/atmos11090959

Eglinton, G., and Hamilton, R.J., 1967. Leaf epicuticular waxes. Science, 156, 1322–1335.

Farquhar, G.D., Ehleringer, J.R., Hubick, K.T., 1989. Carbon isotope discrimination and photosynthesis. Annual Reviews, Plant Physiology, 40, 503–537.

Feakins, S.J., 2013. Pollen-corrected leaf wax D/H reconstructions of northeast African hydrological changes during the late Miocene. Palaeogrography, Palaeoclimatology, Palaeoecology, 374, 62–71.

Fensterer, C., Scholz, D., Hoffmann, D., Spötl, C., Pajón, J.M., Mangini, A., 2012. Cuban stalagmite suggests relationship between Caribbean precipitation and the Atlantic Multidecadal Oscillation during the past 1.3 ka. The Holocene, 22, 1405–1412.

Fensterer, C., Scholz, D., Hoffmann, D., L., Spötl, C., Schröder-Ritzrau, A., Horn, C., Pajón, J.M., Mangini, A., 2013. Millennial-scale climate variability during the last 12.5 ka recorded in a Caribbean speleothem. Earth and Planetary Science Letters, 361, 143–151.

George, R.K., Waylen, P., Laporte, S., 1998. Interannual variability of annual streamflow and the Southern Oscillation in Costa Rica. Hydrological Sciences Journal, 43:3, 409–424.

Giannini, A., Cane, M.A., Kushnir, Y., 2001. Interdecadal changes in the ENSO teleconnection to the Caribbean region and the North Atlantic Oscillation. Journal of Climate, 14, 2867–2879.

Goldsmith, Y., Polissar, P.J., deMenocal, P.B., Broecker, W.S., 2019. Leaf wax δD and $\delta^{13}C$ in soils record hydrological and environmental information across a climate gradient in Israel. Journal of Geophysical Research: Biogeosciences, 124, 2898–2916.

Hastenrath, S. L., and Heller, L., 1977: Dynamics of climatic hazards in northeast Brazil. Quarterly Journal of the Royal Meteorological Society, 103, 77–92.

Hastenrath, S.L., and Lamb, P.J., 1977. Climatic atlas of the tropical Atlantic and eastern Pacific Oceans. The University of Wisconsin Press, Madison, WI.

Hattersley, P.W., 1982. $\delta^{13}C$ values of C_4 types in grasses. Australian Journal of Plant Physiology, 9, 139–154.

Haug, G.H., Hughen, K.A., Sigman, D.M., Peterson, L.C., Röhl, U., 2001. Southward migration of the Intertropical Convergence Zone through the Holocene. Science, 293, 1304–1308.

Haug, G.H., Günnther, D., Peterson, L.C., Sigman, D.M., Hughen, K.A., Aeschlimann, B., 2003.Climate and the collapse of Maya civilization. Science, 299, 1731–1735.

Hidalgo, H.G., Alfaro, E.J., Amador, J.A., Bastidas, A., 2019. Precursors of quasi-decadal dry-spells in the Central America Dry Corridor. Climate Dynamics, 53, 1307–1322.

Hodell, D.A., Curtis, J.H., Brenner, M., 1995. Possible role of climate in collapse of Classic Maya civilization. Nature, 375, 391–394.

Hodell, D.A., Brenner, M., Curtis, J.H., Guilderson, T., 2001. Solar forcing of drought frequency in the Maya lowlands. Science, 292, 1367–1370.

Hodell, D.A., Brenner, M., and Curtis, J.H., 2005. Terminal Classic Drought in the northern Maya lowlands inferred from multiple sediment cores in Lake Chichancanab (Mexico). Quaternary Science Reviews, 24, 1413–1427.

Horn, S.P., 2006. Pre-Columbian maize agriculture in Costa Rica: pollen and other evidence from lake and swamp sediments. In: Staller J.E., Tykot R.H., and Benz B.F. (eds) *Histories of Maize: Multidisciplinary Approaches to the Prehistory, Biogeography, Domestication, and Evolution of Maize*. Amsterdam: Academic Press, 367–380.

Horn, S.P., and Haberyan K.A., 2016. Lakes of Costa Rica. In: Kappelle M (ed) Costa Rican Ecosystems. Chicago: University of Chicago Press, 656–682.

Hurrell, J.W., 1995. Decadal Trends in the North Atlantic Oscillation: Regional Temperatures and Precipitation. Science, 269, 676–679.

Hurrell, J.W., Deser, C., Phillips, A.S., 2019. North Atlantic Oscillation (NAO). Encyclopedia of Ocean Sciences (3rd Edn), 447–454.

Instituto Meteorólogico Nacional. N.d. Precipitación Promedio Anual en Costa Rica, 1961–1980. Escala 1:1,600,000. https://www.imn.ac.cr/web/imn/atlas-climatologico

Johanson, E.N., Horn, S., Lane, C., 2019. Pre-Columbia agriculture, fire, and Spanish contact: a 4200-year record from Laguna Los Mangos, Costa Rica. The Holocene, 29, 1743–1757.

Johanson, E.N., Horn, S.P., Lane, C.S., Sánchez, M., Cecil, J.A., 2020. In Press. Fire history across the Little Ice Age in southern Pacific Costa Rica. Accepted for publication by the Journal of Paleoliminology.

Kaushal, S., and Binford M.W., (1999) Relationship between C:N ratios of lake sediments, organic matter sources, and historical deforestation in Lake Pleasant, Massachusetts, USA. Journal of Paleolimnology 22: 439–442.

Kennett, D., Breitenbachm, S.F.M., Aquino, V.V., Asmerom, Y., Awe, J., Baldini, J.U.L., Bartlein, P., Culleton, B.J., Ebert, C., Jazwa, C., Macri, M.J., Marwan, N., Polyak, V., Prufer, K.M., Ridley, H.E., Sodemann, H., Winterhalder, B., Haug, G.H., 2012. Development and disintegration of Maya political systems in response to climate change. Science, 338, 788–791.

Kerr, M.T., 2019. Holocene precipitation variability, prehistoric agriculture, and natural and human-set fires in Costa Rica. PhD Thesis, University of Tennessee, Knoxville, USA.

Kerr, M.T., Horn, S.P., Lane, C.S., 2020. Stable isotope analysis of vegetation history and land use change at Laguna Santa Elena in southern Pacific Costa Rica. Vegetation History and Archaeobotany, 29, 477–492.

Koutavas, A., deMenocal, P.B., Olive, G.C., Lynch-Stieglitz, J., 2006. Mid-Holocene El Niño Southern Oscillation (ENSO) attenuation revealed by individual foraminifera in eastern tropical Pacific sediments. Geology, 34, 993–996.

Krishnaswamy, J., Halpin, P.H., Richter, D.D., 2001. Dynamics of sediment discharge in relation to land-use and hydro-climatology in a humid tropical watershed in Costa Rica. Journal of Hydrology, 253, 91–109.

Lachniet, M.S., Burn, S.J., Piperno, D.R., Asmerom, Y., Polyak, V.J., Moy, C.M., Christenson, K., 2004. A 1500-year El Niño/Southern Oscillation and rainfall history for the Isthmus of Panama from speleothem calcite. Journal of Geophysical Research, 109, 1–8.

Lachniet, M.S., Bernal, J.P., Asmerom, Y., Polyak, V., Piperno, D., 2012. A 2400 yr Mesoamerican rainfall reconstruction links climate and cultural change. Geology, 40, 259–262.

Lane, C.S., Horn, S.P., and Mora, C.I., 2004. Stable carbon isotope ratios in lake and swamp sediments as a proxy for prehistoric forest clearance and crop cultivation in the Neotropics. Journal of Paleolimnology, 32, 375–381.

Lane, C.S., Horn, S.P., Taylor, Z.P., Mora, C.I., 2009,a. Assessing the scale of prehistoric human impact in the neotropics using stable carbon isotope analyses of lake sediments: a test case from Costa Rica. Latin American Antiquity, 20, 120–133.

Lane, C.S., Horn, S.P., Mora, C.I., Orvis, K.H., 2009,b. Late-Holocene paleoenvironmental change at mid-elevation on the Caribbean slope of the Cordillera Central, Dominican Republic: a multi-site, multi-proxy analysis. Quaternary Science Reviews, 28, 2239–2260.

Lane, C.S., Horn, S.P., Orvis, K.H., Thomason, J.M., 2011,a. Oxygen isotope evidence ofLittle Ice Age aridity on the Caribbean slope of the Cordillera Central Dominican Republic. Quaternary Research, 75, 461–470.

Lane, C.S., Horn, S.P., Mora, C.I., Orvis, K.H., Finkelstein, D.B., 2011,b. Sedimentary stable carbon isotope evidence of late Quaternary vegetation and climate change in highland Costa Rica. Journal of Paleolimnology, 45, 323–338.

Lane, C.S., and Horn, S.P., 2013. Terrestrially derived n-alkane δD evidence of shifting Holocene paleohydrology in highland Costa Rica. Arctic, Antarctic, and Alpine Research, 45, 342–349.

Lane, C.S., Horn, S.P., and Kerr, M.T., 2014. Beyond the Mayan Lowlands: impacts of the Terminal Classic Drought in the Caribbean Antilles. Quaternary Science Reviews, 86, 89–98.

Lane, C.S., Horn, S.P., Taylor, Z.P., Kerr, M.T., 2016. Correlation of bulk sedimentary and compound-specific $\delta^{13}C$ values indicates minimal pre-again of *n*-alkanes in small tropical watershed. Quaternary Science Reviews, 145, 238–242.

930 Lane, C.S., Taylor, A.K., Spencer, J., Jones, K.B., 2018. Compound-specific isotope records of
931 the late-quaternary environmental change in southeastern North Carolina. Quaternary
932 Science Reviews, 182, 48–64.
933
934 Lund, D.C., Lynch-Stieglitz, J., Curry, W.B., 2006. Gulf Stream density structure and transport
935 during the past millennium. Nature Letters, 444, 601–604.
936
937 Magaña, V., Amador, J,A, Medina, S., 1999. The midsummer drought over Mexico and Central
938 America. Journal of Climate, 12, 1577–1588.
939
940 Magrin et al., 2014. Central and South America. In: Climate Change 2014: impacts, adaptation,
941 vulnerability. Part B: regional aspects. Contributions of the Working Group II to the fifth
942 assessment report of the Intergovernmental Panel on Climate Change, 1499–1566.
943
944 Markgraf, V., Baumgartner, T.R., Bradbury, J.P., Diaz, H.F., Dunbar, R.B., Luckman, B.H.,
945 Seltzer, G.O., Swetnam, T.W., Villalba, R., 2000. Paleoclimate reconstruction along the
946 Pole- Equator-Pole transect of the Americas (PEP 1). Quaternary Science Reviews 19,
947 125–140.
948
949 Martinez, N.C., Murray, R.W., Thunell, R.C., Peterson, L.C., Muller-Karger, F., Astor, Y.,
950 Varela, R., 2007. Modern climate forcing of terrigenous deposition in the tropics (Cariaco
951 Basin, Venezuela). Earth and Planetary Science Letters, 264, 438–451.
952
953 Marzi, R., Torkelson, B.E., Olson, R.K., 1993. A revised carbon preference index. Organic
954 Geochemistry, 20, 867–900.
955
956 Meyers, P.A., and Ishiwatari, R., 1993. Lacustrine organic geochemistry- an overview of
957 indicators of organic matter sources and diagenesis in lake sediments. Organic
958 Geochemistry, 20, 867–900.
959
960 Moy, C.M., Seltzer, G.O., Rodbell, D. T., Anderson, D.M., 2002. Variability of El
961 Niño/Southern Oscillation activity at millennial timescales during the Holocene epoch.
962 Nature, 420, 162–165.
963
964 Nobre, P., and Shukla, J., 1996. Variations of sea surface temperature, wind stress, and rain fall
965 over the tropical Atlantic and South America. Journal of Climate, 9, 2464–2479.
966
967 Nyberg, J., Kuijpers, A., Malmgren, B.A., Kunzendorf, H., 2001. Late Holocene changes in
968 precipitation and hydrography recorded in marine sediments from the northeastern
969 Caribbean Sea. Quaternary Research, 56, 87–102.
970
971 Oglesby, R.J., Sever, T.L., Saturno, W., Erickson, D.J., Srikishen, J., 2010. Collapse of the
972 maya: could deforestation have contributed? Journal of Geophysical Research:
973 Atmospheres, 115, D12106.
974

975 Peterson, L.C., Haug, G.H., 2005. Variability in the mean latitude of the Atlantic intertropical
976 convergence zone as recorded by riverine input of sediments to the Cariaco Basin
977 (Venezuela). Palaeogeography, Palaeoclimatology, Palaeoecology, 1–17.
978
979 Polissar, P.J., Abbott, M., Wolfe, A.P., Bezada, M., Rull, V., Bradley, R.S., 2006. Solar
980 modulation of Little Ice Age climate in the tropical Andes. Proceedings of the National
981 Academy of Sciences of the United States of America 103, 8937–8942.
982
983 Polissar, P.J., and D'Andrea, W.J., 2014. Uncertainty in paleohydrologic reconstructions from
984 molecular δD values. Geochimica et Cosmochimica Acta, 129, 146–156.
985
986 Poveda, G., and Mesa, O.J., 1997: Feedbacks between hydrological processes in tropical South
987 America and large-scale ocean–atmospheric phenomena. Journal of Climate, 10, 2690–
988 2702.
989
990 Pulwarty, R.S., and Diaz, H.F., 1993. A study of the seasonal cycle and its perturbation by
991 ENSO in the tropical Americas. IV International Conference on Southern Hemisphere
992 Meteorology and Oceanography, American Meteorological Society, 262–262.
993
994 Rasmusson, E.M., and Carpenter, T.H., 1982. Variations in tropical sea surface temperature and
995 surface wind fields associated with the Southern Oscillation/El Niño, Monthly Weather
996 Review, 110, 354–384.
997
998 Raynor, G.S., Ogden, E.C., and Hayes, J.V., 1972. Dispersion and deposition of corn pollen from
999 experimental sources. Agronomy Journal, 64, 420–427.
1000
1001 Richey, J.N., Poore, R.Z., Flower, B.P., Quinn, T.M., 2007. 1400 yr multiproxy record of climate
1002 variability from the northern Gulf of Mexico. Geology, 35, 423–426.
1003
1004 Rodysill, J.R., Russell, J.M., Vuille, M., Dee, S., Lunghino, B., Bijaksana, S., 2019. La Niña
1005 driven flooding in the Indo-Pacific warm pool during the past millennium. Quaternary
1006 Science Reviews, 225, 1–11.
1007
1008 Ropelewski, C.F., and Halpert, M.S., 1987. Global and regional scale precipitation patterns
1009 associated with the El Niño / Southern Oscillation. Climate Analysis Center/ National
1010 Meteorological Center, NWS/NOAA, monthly weather review, 115, 1606–1626.
1011
1012 Ropeleski, C.F., and Halpert, M.S., 1996: Quantifying Southern Oscillation–precipitation
1013 relationships. Journal of Climate, 9, 1043–1059.
1014
1015 Rosenmeier, M.F., Hodell, D.A., Brenner, M., Curtis, J.H., Martin, J.B., Anselmetti, F.S.,
1016 Ariztegui, D., Guilderson, T.P., 2002. Influence of vegetation change on watershed
1017 hydrology: implications for paleoclimatic interpretation of lacustrine $\delta^{18}O$ records.
1018 Journal of Paleolimnology, 27, 117–131.
1019

Sachs, J.P., Sachse, D., Smittenberg, R.H., Zhang, Z., Battisti, D.S., Golubic, S., 2009. Southward movement of the Pacific intertropical convergence zone AD 1400–1850. Nature Geoscience, DOI: 10.1038/NGEO554.

Sachs, J.P., Mügler, I., Sachse, D., Prebble, M., Wolhowe, M., 2021. Last millennium hydroclimate in the central equatorial North Pacific (5°N, 160°W). Quaternary Science Reviews, 256, 106906.

Sachse, D., Radke, J., Gleixner, G., 2006. δD values of individual *n*-alkanes from terrestrial plants along a climatic gradient- Implications for sedimentary biomarker record. Organic Geochemistry, 37, 469– 483.

Sachse, D., Billault, I., Bowen, G.J., Chikaraishi, Y., Dawson, T.E., Feakins, S.J., Freeman, K.H., Magill, C.R., McInerne, F.A., van der Meer, M.T.J., Polissar, P., Robins, R.J., Sachs, J.P., Schmidt, H.L., Sessions, A.L., White, J.W.C., West, J.B., Kahmen, A., 2012. Molecular Paleohydrology: Interpreting the hydrogen isotopic composition of lipid biomarkers from photosynthesizing organisms. Annual Review of Earth and Planetary Sciences, 40, 221–249.

Sánchez-Murillo, R., Birkel, C., Welsh, K., Esquivel-Hernández, G., Corrales Salazar, J., Boll, J., Brooks, E., Roupsard, O., Sáenz-Rosales, O., Katchan, I., Arce-Mesén, R., Soulsby, C., Araguás-Araguás, L.J., 2016. Key drivers controlling stable isotope variations in daily precipitation of Costa Rica: Caribbean Sea versus Eastern Pacific Ocean moisture sources. Quaternary Science Reviews, 131, 250–261.

Sarachik, E.S., and Cane, M.A. *The El Niño-Southern Oscillation Phenomenon*, Cambridge University Press, 2010. *ProQuest Ebook Central*, https://ebookcentral.proquest.com/lib/miami/detail.action?docID=501290.

Schneider, T., Hampel, H., Mosquera, P.V., Tylmann, W., and Grosjean, M., 2018. Paleo-ENSO revisted: Ecuadorian Lake Pallcacohca does not reveal a conclusive El Niño signal. Global and Planetary Change, 168, 54–66.

Shindell, D.T., Schmidt, G.A., Mann, M.E., Rind, D., Waple, A., 2006. Solar forcing of regional climate change during the Maunder Minimum. Science, 294, 2149–2152.

Sigl, M., Winstrup, M., McConncell, J., Welten, K., Plunkett, G., Ludlow, F., Büntgen, U., Caffee, M., Chellman, N., Dahl-Jensen, D., et al., 2015. Timing and climate forcing of volcanic eruptions for the past 2500 years. Nature, 523, 543–549.

Snarskis, M.J., 1981. The archaeology of Costa Rica. In: Abel-Vidor S and Bakker (eds) Between Continents, Between Seas. New York: Harry N. Abrams, Inc., 15–84.

Stansell, N.D., Steinman, B.A., Abbott, M.B., Rubinov, M., Roman-Lacayo, M., 2013. Lacustrine stable isotope record of precipitation changes in Nicaragua during the Little Ice Age and Medieval Climate Anomaly. Geology, 41, 151–154.

Stuiver, M., Braziunas, T.F., 1989. Atmospheric 14C and century-scale solar oscillations. Nature, 338, 405–407.

Taylor, Z.P., Horn, S.P., and Finkelstein, D.B., 2013. Maize pollen concentrations in Neotropical lake sediments as an indicator of the scale of prehistoric agriculture. The Holocene, 23, 78–84.

Taylor, Z.P., Lane, C.S., Horn, S.P. 2020. A 3600-year record of drought in south Pacific Costa Rica. Quaternary Research, 98, 36–48.

Thompson, L.G., Mosley-Thompson, E., Brecher, H., Davis, M., Leon, B., Les, D., Lin, P.N., Mashiotta, T., Mountain, K., 2006. Abrupt tropical climate change: past and present. Proceedings of the National Academy of Sciences of the United States of America, 103, 10536–10543.

Vargas, A.B., and Trejos, V.F.S., 1994. Changes in the general circulation and its influence on precipitation trends in Central America: Costa Rica. Ambio, 23, 87–90.

Wang, C., 2007. Variability of the Caribbean Low-Level Jet and its relations to climate. Climate Dynamics, 29, 411–422.

Wang, B., Wang, Y., 1999. Dynamics of the ITCZ-equatorial cold tongue complex and causes of the latitudinal climate asymmetry. Journal of Climate, 12, 1830–1847.

Watanabe, T., Winter, A., Oba, T., 2001. Seasonal changes in sea surface temperature and salinity during the Little Ice Age in the Caribbean Sea deduced from Mg/Ca and $^{18}O/^{16}O$ ratios in corals. Marine Geology, 173, 21–35.

Waylen, P., and Laporte, M.S., 1999. Flooding and the El Niño-Southern Oscillation phenomenon along the Pacific coast of Costa Rica. Hydrological Processes, 13, 2623–2638.

Waylen, P.R., Quesada, M.E., Caviedes, C.N., 1996. Temporal and spatial variability of annual precipitation in Costa Rica and the Southern Oscillation. International Journal of Climatology, 16, 173–193.

Webster, J.W., Brook, G.A., Railsback, L.B., Cheng, H., Edwards, R.L., Alexander, C., Reeder, P.P., 2007. Stalagmite evidence from Belize indicating significant droughts at the time of Preclassic Abandonment, the Maya Hiatus, and the Classic Maya collapse. Palaeogeography, Palaeoclimatology, Palaeoecology, 250, 1–17.

Winter, A., Ishioroshi, H., Watanabe, T., Oba, T., Christy, J., 2000. Caribbean sea surface temperatures: two-to-three degrees cooler than present during the Little Ice Age. Geophysical Research Letters, 27, 3365–3368.

Wu., J., Porinchu, D.F., Horn, S.P., 2017. A chironomid-based reconstruction of late-Holocene climate and environmental change for southern Pacific Costa Rica. The Holocene, 27, 73–84.

Wu, J., Porinchu, D.F., Horn, S.P., 2019. Late Holocene hydroclimate variability in Costa Rica: Signature of the terminal classic drought and the Medieval Climate Anomaly in the northern tropical Americas. Quaternary Science Reviews 215, 144–159.

Figure legends

Figure 1. Location of Laguna Los Mangos and other paleolimnological sites in the Diquís archaeological region of Costa Rica, modified from Johanson et al. (2019) (top). Location of Los Mangos in comparison to other Pacific-based paleo δ^2H records (Sachs et al., 2009) and the general latitudinal migration range of the ITCZ during the Northern Hemisphere summer and winter (Haug et al., 2003). The Northern Hemisphere summer (winter) position of the ITCZ generally represents the position of the ITCZ during a cold (warm) ENSO event due to an increase (decrease) in the cross-equatorial SST gradient (bottom).

Figure 2. Radiocarbon age-depth model for the Los Mangos sedimentary record developed using the Clam age-depth modeling program (after Johanson et al., 2019).

Figure 3. Los Mangos proxies after Johanson et al. (2019): pollen (Poaceae, Melastomataceae/Combretaceae and *Ficus)*, charcoal area influx, percent organic matter (%OM), organic carbon to organic nitrogen ratio (C/N ratio), carbon isotope composition of the bulk sediment ($\delta^{13}C_{TOC}$), nitrogen isotope composition of the bulk sediment ($\delta^{15}N_{bulk}$), and presence of maize in the sediment record. The Poaceae curve provides a signal of the replacement of C_3 forest vegetation with herbaceous vegetation or crops that include more C_4 plants, indicating land clearance or possibly climate change, while Melastomataceae/Combretaceae and *Ficus* represent C_3 forest taxa. The solid horizontal lines indicate the timing of the first evidence of maize agriculture in the Los Mangos watershed and of the arrival of the Spanish. The grayscale gradation zone represents the timing of the TCD and LIA at 1200 cal yr BP to 850 cal yr BP and 550 cal yr BP to 100 cal yr BP, respectively. The TCD and LIA records are interrupted by a hiatus in the sediment profile from ca. 950 cal yr BP to 450 cal yr BP. Error bars represent one standard deviation of replicate analyses.

Figure 4. Raw δ^2H_{C29} values in comparison to ε-corrected δ^2H_{C29} values for the Los Mangos record. The dashed lines indicate the hiatus in the sediment profile from ca. 950–450 cal yr BP. The vertical lines extending through both proxies represent the mean value of each proxy for the entire record and are used to determine significant deviations from normal precipitation conditions.

Figure 5**.** Compound-specific carbon and hydrogen isotope proxies from terrestrially derived *n*-alkanes of the Los Mangos sediment record (this study) compared to existing Los Mangos proxies (Johanson et al., 2019). The two horizontal lines drawn across the profiles represent the timing of the earliest evidence of maize agriculture in the Los Mangos watershed and the arrival of the Spanish. The gray shaded zones represent the timing of the TCD and LIA at 1200 cal yr BP to 850 cal yr BP and 550 cal yr BP to 100 cal yr BP, respectively. The TCD and LIA are interrupted by a hiatus in the sediment profile indicated by dashed lines from ca. 950 cal yr BP to 450 cal yr BP. The vertical lines extending through compound-specific proxies (this study) represent the mean value of each proxy for the entire record and are used to determine significant deviations from normal conditions. Error bars (where applicable) represent one standard deviation from duplicate analyses.

Figure 6. Compound-specific hydrogen isotopic values of C_{29} *n*-alkanes at Laguna Los Mangos (this study), and δ^2H records from Washington Lake, Spooky Lake, and El Junco Lake from Sachs et al. (2009) compared to percent Ti (%Ti) from the Cariaco Basin site ODP 1002 (Haug et al., 2001, 2003). Haug et al. (2001, 2003) related increased (decreased) amounts of %Ti deposited in the Cariaco Basin to increased (decreased) precipitation. The vertical lines extending through each record represent the mean value of each proxy for the entire record and are used to determine significant deviations from normal precipitation conditions. The dashed line between δ^2H_{C29} Los Mangos data points indicate a hiatus in the sediment profile. The gray shaded zones represent the timing of the TCD and LIA at 1200 cal yr BP to 850 cal yr BP and 550 cal yr BP to 100 cal yr BP, respectively. The light gray box on the TLE δ^2H Washington Lake record represents the timing of the most arid conditions as compared to the entire record indicated by increased δ^2H values and dominance of salt-tolerant cyanobacteria (*Aphanothece*).

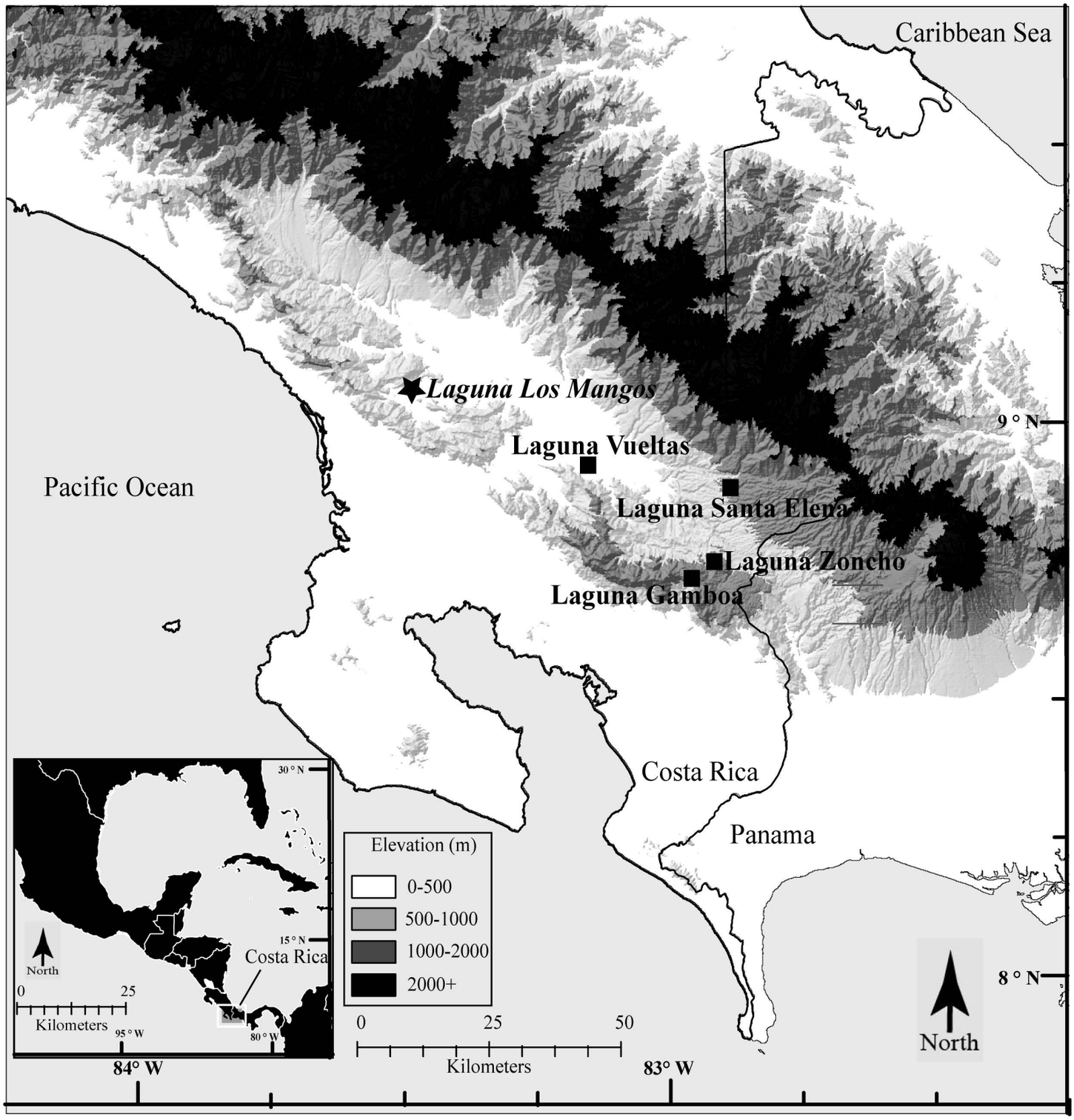
Caribbean Sea
Laguna Los Mangos
Laguna Vueltas
Laguna Santa Elena
Laguna Zoncho
Laguna Gamboa
Pacific Ocean
Costa Rica
Panama
9 ° N
8 ° N
84° W
83° W
North
Elevation (m)
0-500
500-1000
1000-2000
2000+
0
25
50
Kilometers
30 ° N
15 ° N
95 ° W
80 ° W
Costa Rica
North
0
25
Kilometers

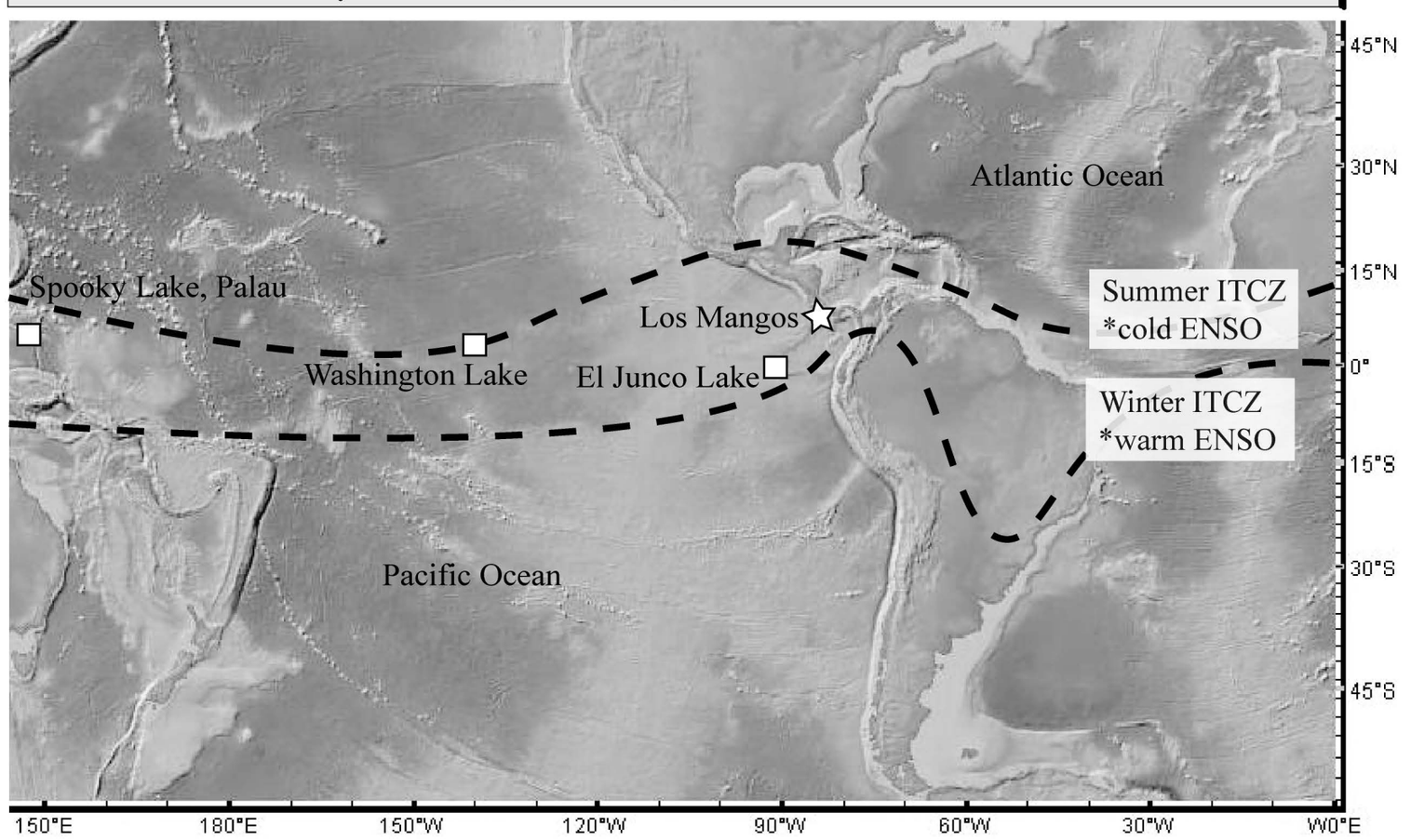
Atlantic Ocean
Spooky Lake, Palau
Los Mangos
Washington Lake
El Junco Lake
Summer ITCZ
*cold ENSO
Winter ITCZ
*warm ENSO
Pacific Ocean
45°N
30°N
15°N
0°
15°S
30°S
45°S
150°E
180°E
150°W
120°W
90°W
60°W
30°W
W0°E

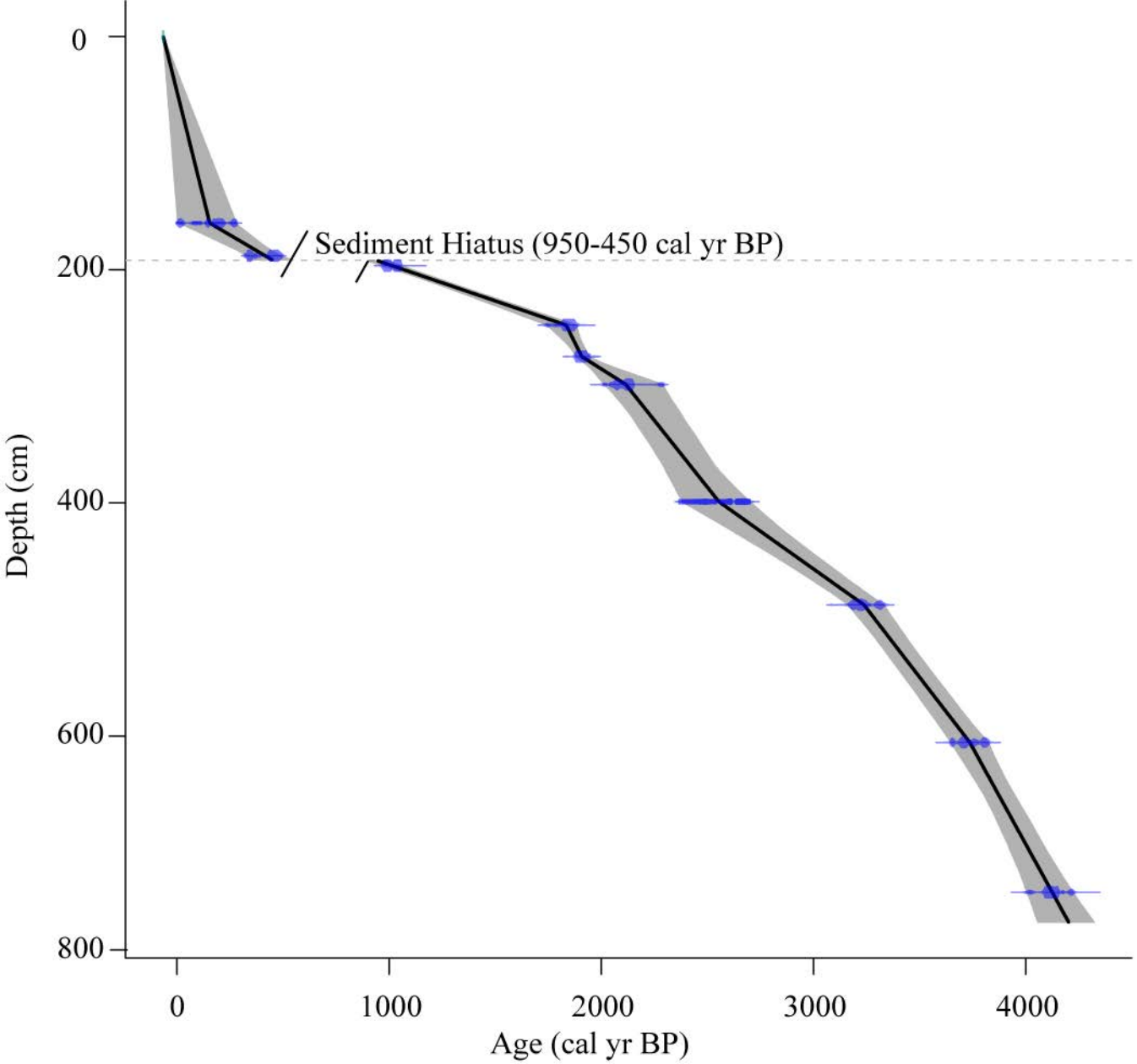
0
200
400
600
800
Depth (cm)
Sediment Hiatus (950-450 cal yr BP)
0
1000
2000
3000
4000
Age (cal yr BP)

Depth (cm)
Poaceae
Melastomataceae/Combretaceae
Ficus
Charcoal Area Influx
% OM
C/N Ratio
$\delta^{13}C_{TOC}$
$\delta^{15}N_{bulk}$
Maize Presence
LIA
Spanish Contact
TCD
Sediment Hiatus
Maize Agriculture
Age (cal yr BP)
% Total Pollen
% Total Pollen
% Total Pollen
mm/cm²/yr
% Organic Matter
‰VPDB
‰ AIR
Bar = Present

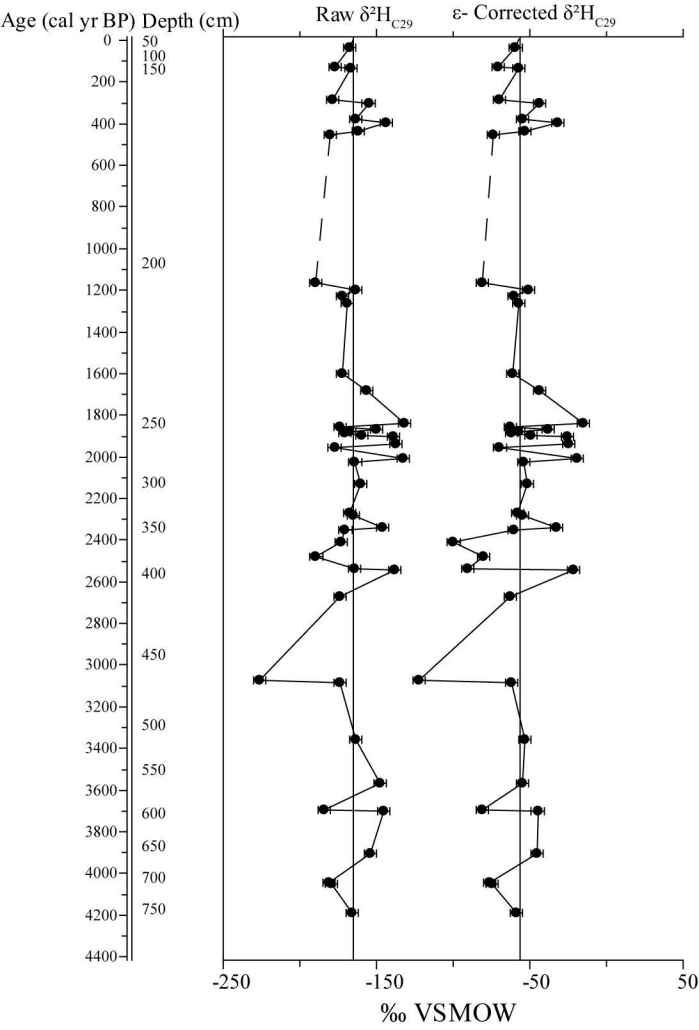
Age (cal yr BP)
Depth (cm)
Raw δ²H_C29
ε- Corrected δ²H_C29
0
200
400
600
800
1000
1200
1400
1600
1800
2000
2200
2400
2600
2800
3000
3200
3400
3600
3800
4000
4200
4400
50
100
150
200
250
300
350
400
450
500
550
600
650
700
750
-250
-150
-50
50
‰ VSMOW

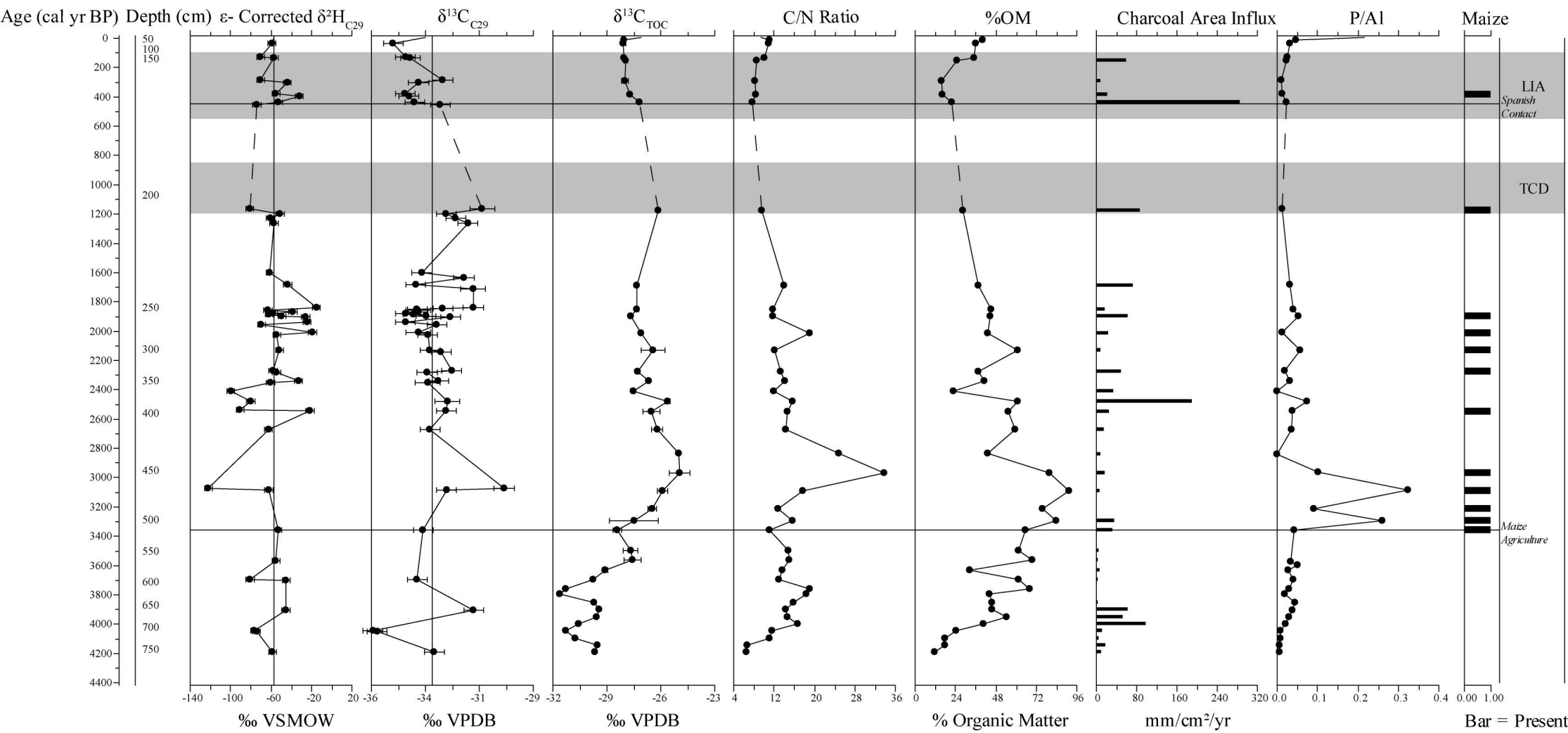
Age (cal yr BP)
Depth (cm)
ε- Corrected δ²H C29
δ13C C29
δ13C TOC
C/N Ratio
%OM
Charcoal Area Influx
P/Al
Maize
LIA
Spanish Contact
TCD
Maize Agriculture
‰ VSMOW
‰ VPDB
‰ VPDB
% Organic Matter
mm/cm²/yr
Bar = Present

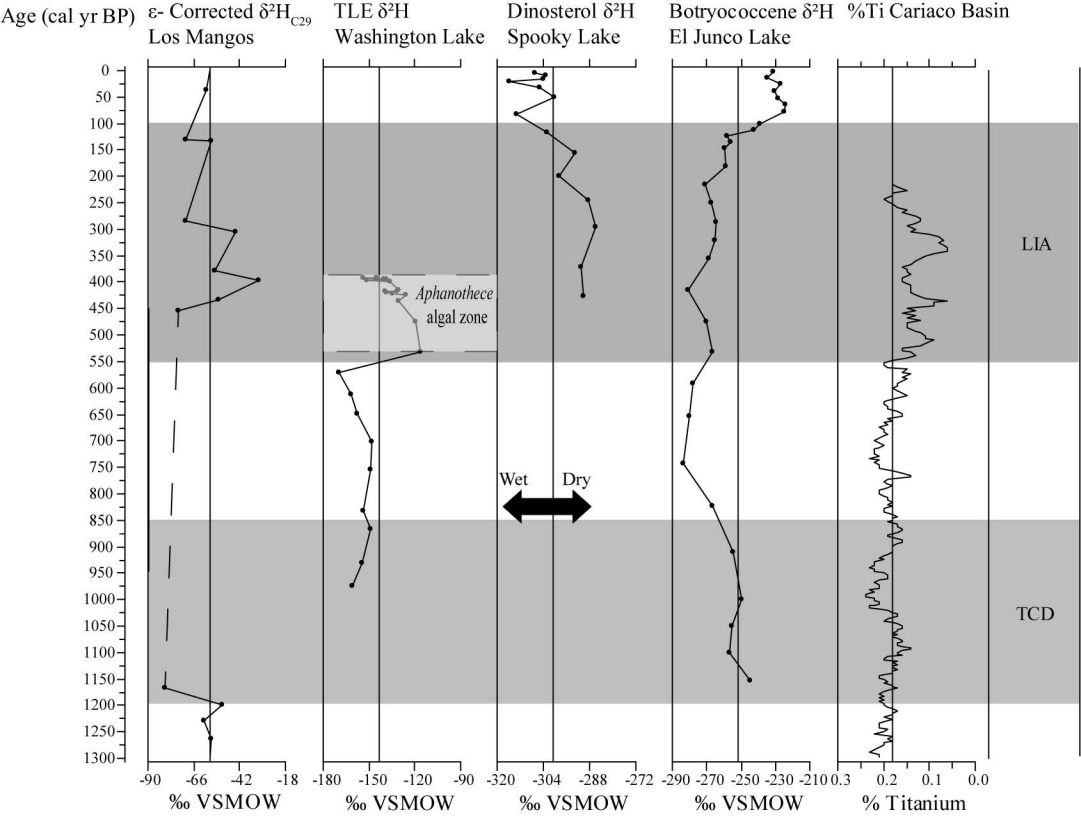
Age (cal yr BP)
ε- Corrected δ²H$_{C29}$
Los Mangos
TLE δ²H
Washington Lake
Dinosterol δ²H
Spooky Lake
Botryococcene δ²H
El Junco Lake
%Ti Cariaco Basin
Aphanothece
algal zone
Wet
Dry
LIA
TCD
‰ VSMOW
‰ VSMOW
‰ VSMOW
‰ VSMOW
% Titanium

Taxa	Life Form Category	ε_{C27}	ε_{C29}	ε_{C31}
Anacardiaceae	Angiosperm tree + shrub	–107‰	–111‰	–107‰
Apocynaceae	Angiosperm tree + shrub	–107‰	–111‰	–107‰
Arecaceae	Angiosperm tree + shrub	–107‰	–111‰	–107‰
Ericaceae	Angiosperm tree + shrub	–107‰	–111‰	–107‰
Malpighiaceae	Angiosperm tree + shrub	–107‰	–111‰	–107‰
Melastomataceae/ Combretaceae	Angiosperm tree + shrub	–107‰	–111‰	–107‰
Mimosoideae (*Mimosa*)	Angiosperm tree + shrub	–107‰	–111‰	–107‰
Myrtaceae	Angiosperm tree + shrub	–107‰	–111‰	–107‰
Rhamnaceae	Angiosperm tree + shrub	–107‰	–111‰	–107‰
Rubiaceae	Angiosperm tree + shrub	–107‰	–111‰	–107‰
Sapindaceae	Angiosperm tree + shrub	–107‰	–111‰	–107‰
Sapotaceae/Meliaceae	Angiosperm tree + shrub	–107‰	–111‰	–107‰
Solanaceae	Angiosperm tree + shrub	–107‰	–111‰	–107‰
Tiliaceae	Angiosperm tree + shrub	–107‰	–111‰	–107‰
Urticales (di- + triporate)	Angiosperm tree + shrub	–107‰	–111‰	–107‰
Acalypha	Angiosperm tree + shrub	–107‰	–111‰	–107‰
Alchornea	Angiosperm tree + shrub	–107‰	–111‰	–107‰
Alfaroa	Angiosperm tree + shrub	–107‰	–111‰	–107‰
Alnus	Angiosperm tree + shrub	–107‰	–111‰	–107‰
Bursera	Angiosperm tree + shrub	–107‰	–111‰	–107‰
Cecropia	Angiosperm tree + shrub	–107‰	–111‰	–107‰
Celtis	Angiosperm tree + shrub	–107‰	–111‰	–107‰
Croton (Euphorbiaceae)	Angiosperm tree + shrub	–107‰	–111‰	–107‰
Ficus	Angiosperm tree + shrub	–107‰	–111‰	–107‰
Hedyosmum	Angiosperm tree + shrub	–107‰	–111‰	–107‰
Ilex	Angiosperm tree + shrub	–107‰	–111‰	–107‰
Iriartea	Angiosperm tree + shrub	–107‰	–111‰	–107‰
Myrica	Angiosperm tree + shrub	–107‰	–111‰	–107‰
Myrsine	Angiosperm tree + shrub	–107‰	–111‰	–107‰
Piper	Angiosperm tree + shrub	–107‰	–111‰	–107‰
Quercus	Angiosperm tree + shrub	–107‰	–111‰	–107‰
Sapium	Angiosperm tree + shrub	–107‰	–111‰	–107‰
Trema	Angiosperm tree + shrub	–107‰	–111‰	–107‰
Ulmus	Angiosperm tree + shrub	–107‰	–111‰	–107‰
Virola (Myristicaceae)	Angiosperm tree + shrub	–107‰	–111‰	–107‰
Weinmannia	Angiosperm tree + shrub	–107‰	–111‰	–107‰
Amaranthaceae	Forb	–124‰	–128‰	–130‰
Apiaceae	Forb	–124‰	–128‰	–130‰
Asteraceae	Forb	–124‰	–128‰	–130‰
Caryophyllaceae	Forb	–124‰	–128‰	–130‰
Cucurbitaceae	Forb	–124‰	–128‰	–130‰
Cyperaceae	Graminoid (C4)	–131‰	–132‰	–136‰
Poaceae	Graminoid (C4)	–131‰	–132‰	–136‰

Zea mays subsp. *mays*	Graminoid (C4)	–131‰	–132‰	–136‰
Mono- and Trilete fern spores	Pteridophytes	–103‰	–108‰	–114‰
Urticales polyporate[1]	Cannot Classify			
Cuphea[2]	Cannot Classify			
Polygalaceae[3]	Cannot Classify			
Violaceae[3]	Cannot Classify			
Acanthaceae[3]	Cannot Classify			

[1] Cannot classify because this group may contain taxa of multiple life forms.

[2] Cannot classify because genus includes annual and perennial herbs, semi-shrubs, and shrubs.

[3] Cannot classify because this family includes herbs, shrubs, and trees.

Sample	Depth (cm)	Age (cal yr BP)	ug/g OM C27	ug/g OM C29	ug/g OM C31	ug/g OM C33	ug/g OM C35	$\delta^{13}C_{C29}$	$\delta^{13}C_{C31}$	$\delta^{2}H_{C29}$	$\delta^{2}H_{C31}$
M1	40	-9	6.64	15.45	18.55	10.18	1.81	-33.2	-33.4	-66.9	-71.9
M2	42	-7	6.65	15.23	16.47	9.41	3.22	-33.4	-33.5	-56.6	-63.9
M4	74	36	6.01	27.32	36.79	19.72	3.87	-35.0	-35.4	-59.1	-64.5
M5	142	130	4.52	26.03	37.38	18.66	2.32	-34.5	-35.0	-70.4	-72.8
M6	144	133	6.99	30.14	39.33	18.37	4.10	-34.3	-34.5	-56.8	-63.1
M7	174	285	0.10	0.67	0.91	0.57	0.12	-32.8	-35.4	-70.2	-70.8
M8	176	304	5.99	29.41	35.94	22.02	4.06	-33.9	-34.1	-43.9	-49.6
M9	184	378	0.12	0.78	1.21	0.84	0.19	-34.5	-34.3	-55.0	
M10	186	397	6.74	32.11	36.81	20.88	5.23	-34.3	-34.3	-32.0	
M11	190	434	4.64	20.92	29.42	19.32	5.76	-34.1	-34.5	-52.8	-53.8
M12	192	453	4.66	14.58	20.39	16.89	8.26	-32.9	-33.0	-74.1	-69.8
M13	206	1166	1.28	2.91	4.47	3.27	1.20	-31.1	-32.9	-81.0	-67.6
M14	208	1198	7.84	15.53	21.46	16.02	4.75	-32.7	-33.7	-51.0	-50.0
M15	210	1230	1.72	3.34	4.60	4.45	1.81	-32.3	-33.3	-60.5	-60.5
M16	212	1263	3.94	8.96	9.68	6.54	2.79	-31.7	-34.0	-57.1	-56.8
M17	233	1601	3.37	10.94	12.45	7.57	2.92	-33.8	-34.2	-61.0	-62.1
M18	235	1633	1.71	4.47	4.82	3.27	2.37	-31.9	-33.0		
M19	238	1681	3.33	13.53	12.82	6.90	2.63	-34.0	-34.3	-43.4	-42.5
M20	240	1713	1.34	1.91	1.87	1.80	1.90	-31.5	-30.9		-96.4
M23	250	1841	0.59	1.87	1.78	1.26	0.67	-31.5	-35.3	-15.1	-12.1
M24	252	1846	0.27	1.25	1.19	0.86	0.51	-32.8	-33.9		
M25	254	1852	1.49	3.89	3.15	2.10	1.50	-34.0	-34.2		
M26	256	1857	2.14	9.73	10.15	6.65	3.58	-33.9	-33.4	-62.8	-63.5
M28	261	1871	3.64	13.41	13.29	9.34	5.65	-33.9	-34.3	-38.4	-48.3
M29	265	1882	3.99	13.99	14.21	9.44	4.77	-34.5	-35.0	-57.5	-53.0
M30	266.5	1886	2.06	5.66	4.74	3.16	1.96	-34.1	-34.3	-61.7	-62.8
M31	270	1895	4.79	17.80	19.76	12.30	5.47	-33.6	-34.2	-49.0	-50.3
M32	272	1901	0.26	1.04	1.07	0.73	0.38	-32.5	-34.3	-25.7	-27.9
M33	278	1938	5.10	27.74	27.88	17.73	8.70	-34.5	-34.7	-24.2	-46.8
M34	280	1955	2.02	7.67	6.91	4.26	2.79	-33.1	-34.1	-69.5	-68.0
M35	286	2007	1.83	11.20	9.25	5.30	3.35	-33.9	-34.3	-19.0	-30.9
M36	288	2025	4.61	22.32	21.21	16.03	9.49	-33.5	-34.7	-54.1	-55.5
M37	302	2131	0.04	0.14	0.19	0.26	0.24	-33.4	-34.6	-51.5	
M38	304	2140	1.10	3.38	3.08	2.22	1.29	-32.9	-33.5		-48.1
M39	334	2270	4.55	16.27	18.23	12.26	5.44	-32.4	-33.5	-57.7	-57.2
M40	336	2279	3.46	11.02	12.18	8.35	3.34	-33.5	-34.1	-54.6	
M41	350	2340	4.59	15.61	12.71	6.62	1.57	-33.0	-34.2	-32.8	-31.2
M42	352	2349	2.42	7.93	5.35	2.76	1.69	-33.5	-33.4	-60.4	
M43	366	2410	0.27	0.64	0.63	0.14	0.14		-34.6	-99.6	
M45	382	2480	1.05	3.04	3.87	4.53	0.85	-32.6	-33.4	-79.8	-73.2
M47	395	2536	0.88	2.22	3.36	3.66	1.28		-33.3	-90.6	-51.9

M48	397	2545	2.36	10.40	10.12	8.08	1.59	-32.7	-35.0	-21.6	-21.6
M49	414	2670	2.63	10.64	12.57	11.58	2.46	-33.4	-34.2	-62.4	-57.4
M52	452	2963	0.02	0.17	0.10	0.14	0.10		-34.4		
M53	466	3071	14.50	16.40	5.79	1.70	1.34	-30.1	-28.9	-121.9	-96.6
M54	468	3087	7.64	31.60	28.97	18.01	7.64	-32.7	-33.7	-62.0	-55.8
M57	516	3358	3.89	8.89	8.93	3.05	0.76	-33.7	-34.0	-53.1	-50.1
M60	566	3569	1.36	2.40	2.70	1.81	1.18		-35.9	-55.1	-35.5
M61	596	3696	2.87	6.85	5.47	2.24	0.27	-34.0	-36.1	-80.7	-80.2
M62	598	3704	5.18	3.12	2.75	2.00	1.58		-35.0	-44.8	-18.1
M64	662	3907	4.67	11.04	10.25	6.42	3.19	-31.5	-32.2	-45.2	-40.6
M65	708.5	4047	3.93	12.12	17.35	8.17	0.99	-35.9	-34.8	-76.2	-75.5
M66	710.5	4053	0.35	1.16	1.76	0.83	0.26	-35.7	-34.7	-74.3	-81.8
M67	755.5	4189	6.51	20.30	27.90	16.37	2.31	-33.2	-34.4	-58.5	-56.4